Dynamic relocalization of the cytosolic type III secretion system components ensures specific protein secretion

Stephan Wimmi[1], Alexander Balinovic[2], Hannah Jeckel[2,3], Lisa Selinger[1], Dimitrios Lampaki[1], Emma Eisemann[1*], Ina Meuskens[4], Dirk Linke[4], Knut Drescher[2,3], Ulrike Endesfelder[2] & Andreas Diepold[1]*

1: Max Planck Institute for Terrestrial Microbiology, Department of Ecophysiology, Karl-von-Frisch-Str. 10, 35043 Marburg, Germany

2: Max Planck Institute for Terrestrial Microbiology, Karl-von-Frisch-Str. 10, 35043 Marburg, Germany

3: Department of Physics, Philipps-Universität Marburg, Karl-von-Frisch-Str. 16, 35043 Marburg, Germany

4: University of Oslo, Department of Biosciences, Blindernveien 31, 0371 Oslo, Norway

* current addresses:

Dimitrios Lampaki, Max-Planck-Institut für Immunbiologie und Epigenetik, Stübeweg 51, 79160 Freiburg, Germany;
Emma Eisemann, James Madison University, 800 South Main St, Harrisonburg, VA 22807, USA

Correspondence: Andreas Diepold, andreas.diepold@mpi-marburg.mpg.de, +49-6421-178302

Running title: Dynamic pH adaptation of the T3SS

Abstract

Many gastrointestinal pathogens use a type III secretion system (T3SS) to manipulate host cells. Protein secretion by the T3SS injectisome is activated upon contact to any host cell, and it has been unclear how premature effector secretion is prevented during infection. We found that at low external pH, such as in the stomach, the components at the proximal interface of the injectisome are temporarily released to the bacterial cytosol, preventing protein secretion. Low external pH is sensed in the periplasm and leads to a partial dissociation of the inner membrane injectisome component SctD, which in turn causes the dissociation of the cytosolic T3SS components. This effect is reversed upon restoration of neutral pH, allowing a fast activation of the T3SS at the native target regions within the host. These findings indicate that the cytosolic components form an adaptive regulatory interface, which regulates T3SS activity in response to environmental conditions.

Introduction

In order to proliferate in contact to eukaryotic host cells, both symbiotic and pathogenic bacteria have developed methods to influence host cell behavior. The type III secretion system (T3SS) injectisome is a molecular machinery used by various pathogenic bacterial genera including *Salmonella, Shigella,* pathogenic *Escherichia* and *Yersinia* to deliver molecular toxins – effector proteins – directly into the eukaryotic host cells. While the effectors differ among the different bacterial species (Büttner, 2012), and can have different functions in modulating the cytoskeleton, invading and escaping host cells or endosomes, or inducing host cell death (Coburn et al., 2007; Hueck, 1998), the structural proteins of the injectisome are highly conserved. An extracellular needle is formed by helical polymerization of a T3SS-exported protein, and ends in a pentameric tip structure. At the proximal end, the needle is anchored by two multimeric membrane rings that span the outer and inner membrane. Additionally, the inner membrane (IM) ring encloses the export apparatus. At the cytosolic interface of the injectisomes, four soluble T3SS components (SctK/Q/L/N)[a] interact to form six pod structures (Hu et al., 2017, 2015) (Fig. 1A).

The soluble T3SS components SctK, SctQ, SctL and SctN interact in a linear fashion (Jackson and Plano, 2000), and the presence of all four proteins is needed for their assembly at the injectisome, and subsequently for effector secretion (Diepold et al., 2017, 2010). SctK/Q/L form a high molecular weight complex that has been shown to bind chaperones and effectors (Lara-Tejero et al., 2011). Since the cytosolic components do not co-purify with the rest of the needle, their structural arrangement has only been revealed by recent *in situ* cryo-electron tomography (Hu et al., 2017, 2015; Nans et al., 2015), which showed the formation of six pod structures at the cytosolic interface of the injectisome. The connection between these pod structures and the membrane rings is established by the cytosolic component SctK, which binds to SctD. In the presence of SctK, the cytosolic domains of SctD ($SctD_C$) rearrange and in the case of the *Salmonella* SPI-1 T3SS form six discrete patches of four $SctD_C$ each that interact with one SctK protein, which in turn connects to SctQ, SctL, and SctN (Hu et al., 2017; Tachiyama et al., 2019).

In addition to forming the injectisome-bound pod structures, the cytosolic components exist in a freely diffusing cytosolic state, with proteins exchanging between the two states (Diepold et al., 2015).

[a] In this manuscript, T3SS refers to the virulence-associated T3SS. The common „Sct“ nomenclature (Hueck, 1998) is used for T3SS components, see (Diepold and Wagner, 2014) for species-specific names.

In the cytosol, SctK/Q/L/N form a dynamic adaptive network, with a variety of complexes of different stoichiometries that change their composition in response to different external conditions (Bernal et al., 2019; Diepold et al., 2017). Strikingly, protein interactions and exchange rates amongst the cytosolic components correlate with the activity of the injectisome (Diepold et al., 2017, 2015; Rocha et al., 2018). However, the precise role of the cytosolic components in the secretion process remains unclear to this date.

Yersinia enterocolitica is an extracellular gastrointestinal pathogen that employs its T3SS to downregulate immune responses and prevent inflammation after the penetration of the intestinal epithelium. For initial attachment to the epithelium, the bacteria employ a number of adhesins, with *Yersinia* adhesin A (YadA) as the key factor for establishing an infection (Meuskens et al., 2019). YadA interacts with a variety of extracellular matrix molecules, including collagen and fibronectin (Mühlenkamp et al., 2015b). YadA length is tightly linked to the length of the injection needle of the T3SS, and establishes close contact to the host cells enabling injection (Mota et al., 2005). *Y. enterocolitica* is usually taken up with contaminated food or water. The shift from environmental to host temperature (37°C) induces expression and assembly of the injectisomes as well as YadA (Cornelis, 2006; Tertti et al., 1992). The bacteria then have to pass the acidic environment of the stomach. During that time, the injectisome can already be present and ready for effector secretion. Since the T3SS readily translocates cargo into any host cell type it adheres to, including immune cells, epithelial cells and even red blood cells (Clerc et al., 1986; Håkansson et al., 1996), a distinct mechanism is needed to prevent premature activation of the T3SS during the passage of the stomach, which would result in a loss of valuable resources, or even elicit immune responses.

We hypothesized that the acidic environment in the stomach (external pH of 1.5 – 4.5 (Evans et al., 1988; McClements and Li, 2010), Fig. 1B) may be detected by the bacteria to inhibit effector secretion under these conditions. Here, we investigated this hypothesis with a combination of fluorescence microscopy, single particle tracking, and functional assays. Our findings show that although parts of the T3SS, including the extracellular needle, are stable at low pH, a set of cytosolic T3SS components temporarily unbind from the injectisome at low external pH. The reversible dissociation corresponds to a temporary suppression of effector secretion by the T3SS. This mechanism prevents premature activation of the T3SS, while ensuring a quick reactivation of the T3SS, once a pH-neutral environment is reached. Our data provide a striking example for how bacteria apply protein dynamics to adapt the function of a large macromolecular machine essential for virulence to external conditions.

Results

Resistance of *Y. enterocolitica* and its T3SS needles to low external pH

To investigate to which degree *Y. enterocolitica* can withstand a drop in external pH, bacterial cultures in exponential growth phase were exposed to different pH for 15 minutes at 28°C, and bacterial survival was monitored by a dilution series on neutral pH agar (Fig. 1C). The results show that *Y. enterocolitica* tolerates temporary incubation down to pH 3, with no or very little fitness decrease at pH 4 and above.

Y. enterocolitica adheres to host cells and other surfaces by adhesins, most importantly the trimeric adhesin YadA, and invasin (Keller et al., 2015; Leo et al., 2015; Mühlenkamp et al., 2015a). We thus tested whether low pH prevents the binding of YadA to collagen and more generally, of *Y. enterocolitica* cells to surfaces. Binding could be established at low pH in both cases (Fig. 1D, Suppl. Movies 1-2). These results suggest that to avoid protein translocation into non-host cells, secretion itself might be prevented at low pH.

To test under which conditions *Y. enterocolitica* secretes effectors, we performed a secretion assay where *Y. enterocolitica* cells primed for secretion were subjected to secreting media in the range from pH 8 to pH 4. Indeed, we observed that effector secretion did not occur at low pH (Fig. 1E). Lack of secretion is not due to lower protein synthesis at pH 4 (Suppl. Fig. 1), suggesting a specific mechanism to suppress secretion at low external pH.

But how does *Y. enterocolitica* prevent secretion at low pH? To determine if the absence of secretion is due to a complete disassembly of injectisomes at that pH, we visualized the needles at different pH values and over time by labeling an introduced cysteine residue with a maleimide-linked dye (Milne-Davies et al., 2019). The needles were stable at pH 4 over continued time periods (Fig. 1F).

Taken together, *Y. enterocolitica* as well as the injectisome needles can withstand low external pH conditions, but still effectors are not secreted.

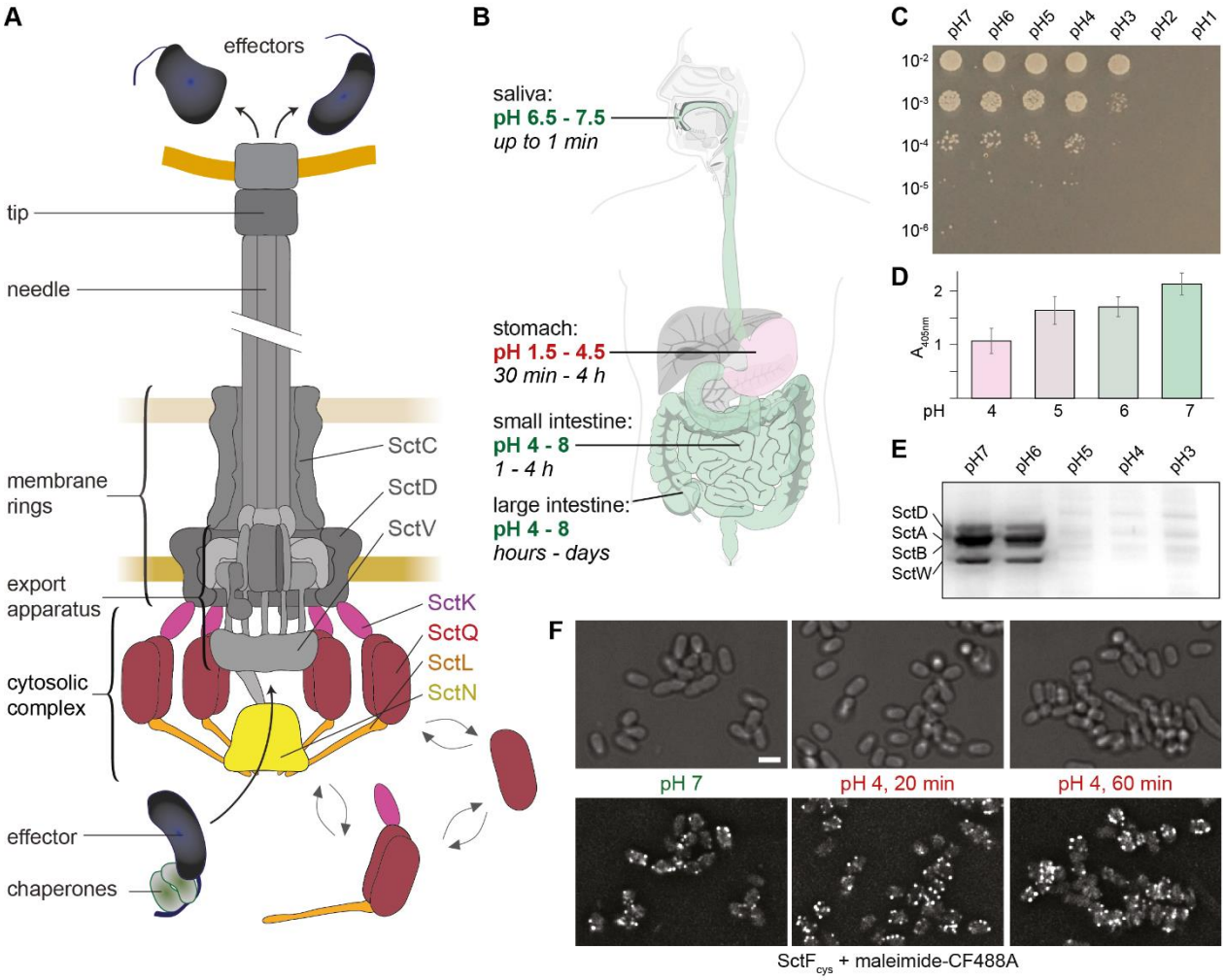

Fig. 1 – The *Yersinia enterocolitica* T3SS and its function and stability at low pH

(**A**) Schematic representation of the active T3SS injectisome (modified from (Diepold and Wagner, 2014)). Left side, description of main substructures; right side, names of T3SS components studied in this manuscript. (**B**) pH ranges and typical retention times at different parts of the gastrointestinal system (Evans et al., 1988; McClements and Li, 2010). Digestive tract image based on the public domain template https://commons.wikimedia.org/wiki/File:Digestive_system_diagram_de.svg. (**C**) Dilution drop test of *Y. enterocolitica* cultures incubated at the indicated pH for 15 minutes. (**D**) Binding of the *Y. enterocolitica* adhesin YadA to collagen at the indicated pH values. Absorption at 405 nm resulting from Ni^{2+}-HRP binding to YadA-His_6 incubated with plate-absorbed calf collagen type I. *n* = 3, error bars denote standard deviation. (**E**) *In vitro* secretion assay showing the export of native T3SS substrates (indicated on left side) at the indicated external pH values. (**F**) Staining of T3SS needles at the different indicated external pH values; time indicates the duration of pH 4 treatment. A strain expressing the mutated needle subunit $SctF_{cys}$ was covalently labeled with maleimide-CF488A. Scale bar, 2 µm.

114 Association of the dynamic cytosolic T3SS components to the injectisome is temporarily suppressed
115 at low external pH

116 We have recently found that the cytosolic T3SS components (SctK/Q/L/N) form a dynamic network,
117 where protein exchange is connected to the function of the injectisome (Fig. 1A) (Diepold et al., 2017,
118 2015). Hence, we wondered whether these dynamic components could be involved in the inhibition
119 of secretion at low pH. To investigate this question, we performed flow-cell-based total internal
120 reflection fluorescence (TIRF) microscopy with functional N-terminal fluorescent protein fusions of
121 the cytosolic components, expressed at native levels[b]: EGFP-SctK, EGFP-SctQ, EGFP-SctL and EGFP-
122 SctN (Fig. 1A) (Diepold et al., 2017, 2010). At neutral or near-neutral pH, the cytosolic components
123 localized in foci at the bacterial membrane, which represent their injectisome-bound state (Diepold
124 et al., 2010). However, at an external pH of 4, all cytosolic components lost this punctuate localization,
125 and the proteins relocated to the cytosol (Fig. 2 ABC). The relocation remained stable over time at low
126 external pH (Suppl. Fig. 2). Strikingly, this phenomenon was reversible: Upon exposure to neutral
127 external pH, the foci recovered within a few minutes (Fig. 2ABC). This effect was observed both under
128 secreting and non-secreting conditions (Suppl. Fig. 3A), and was independent of the fluorophore or
129 visualization tag that was used (Suppl. Fig. 3B). Dissociation and re-association of the cytosolic T3SS
130 components in response to the external pH was reversible in several cycles (Suppl. Movie 3). This
131 reversible response to low pH was also observed both under secreting and non-secreting conditions
132 (presence of 5 mM $CaCl_2$ and EGTA, respectively) (Suppl. Fig. 4).

133 To determine the kinetics of association and dissociation of SctQ, we monitored EGFP-SctQ foci in the
134 flow cell after a pH drop from 7 to 4 and *vice versa*. Foci gradually disappeared within two minutes
135 under secreting condition (Fig. 2D, Suppl. Fig. 5, Suppl. Movie 4). Upon restoration of neutral external
136 pH, the first distinct foci were visible after 50 seconds, and further increased in abundance and
137 brightness over time (Suppl. Fig. 6, Suppl. Movie 5).

138 To test whether the recovery of foci was due to the synthesis of new proteins or if the previously
139 bound proteins rebind to the injectisomes, we covalently labeled the pool of Halo-tagged SctL with
140 the Janelia Fluor JF-646 Halo ligand dye (Grimm et al., 2017) prior to the incubation at pH 4 to ensure
141 that only the protein pool present at the time of labelling was fluorescent. Similar to the previous

[b] All fusion proteins used in this study are expressed from the native genetic environment; the genes replace the wild-type genes by allelic exchange (Kaniga et al., 1991).

experiments, we observed a reversible loss of fluorescent foci at the membrane and an increase in cytosolic signal at pH 4 and rebinding of the fluorescent proteins upon changing pH to 7. Also, an overlay of the micrograph at pH 7 before and after the incubation at pH 4 further indicated that the foci reform at the same position as they previously appeared (Fig. 2E).

Taken together, our data indicate that the cytosolic components reversibly dissociate from the injectisome at low external pH. Upon exposure to neutral pH, proteins from the same pool rebind at the cytosolic interface of the injectisome, forming the potential basis for a regulatory mechanism for the prevention of secretion at low pH.

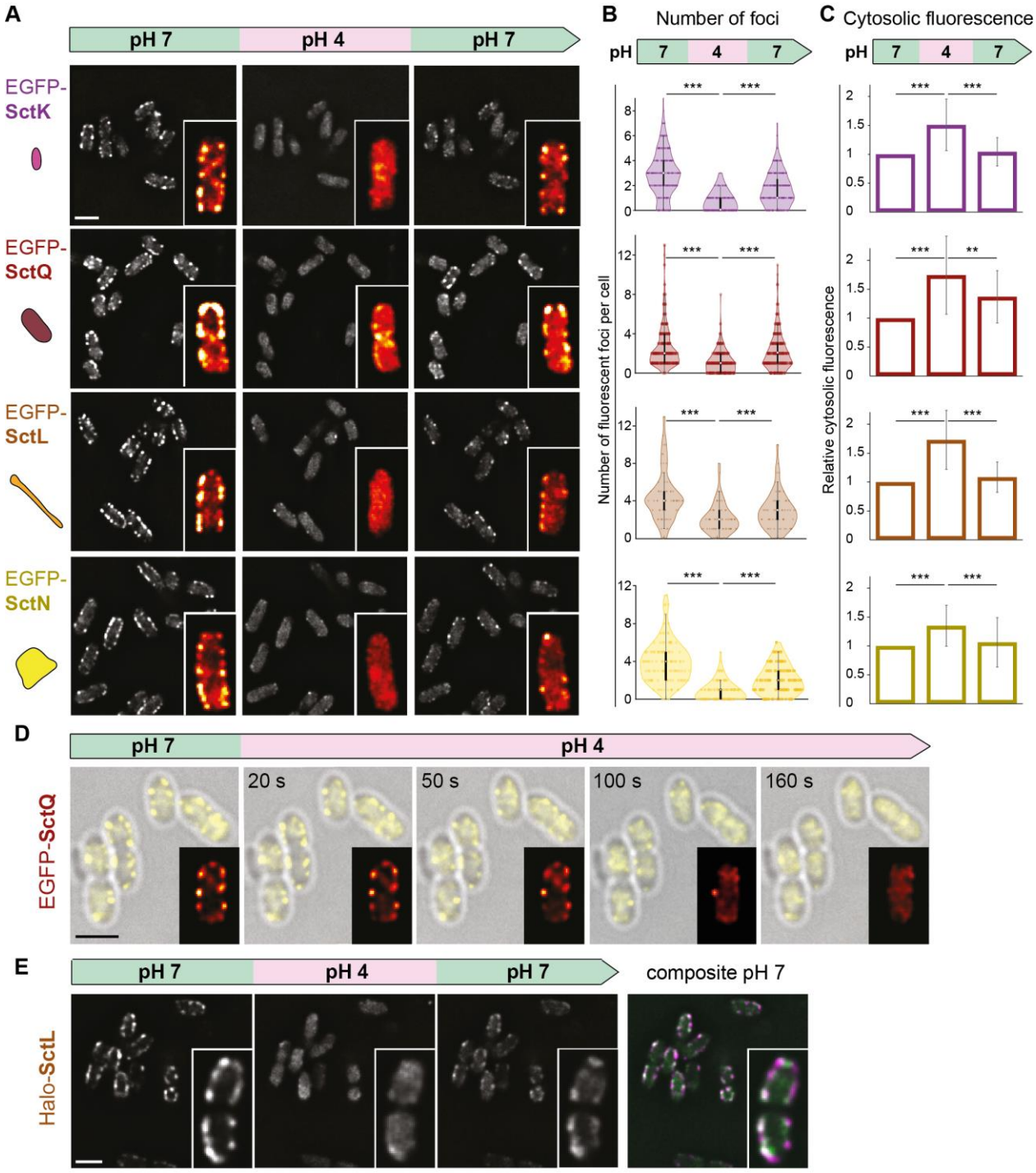

Fig. 2 – The cytosolic T3SS components temporarily dissociate from the injectisome at low external pH

(**A**) Fluorescent micrographs of the indicated proteins in live *Y. enterocolitica*, consecutively subjected to different external pH in a flow cell. Images were taken under secreting conditions, 10 minutes after bacteria were subjected to the indicated pH. Insets, enlarged single bacteria, visualized with the ImageJ red-hot color scale. (**B**) Quantification of foci per bacterium for the strains and conditions shown in panel (A). *n* = 324, 320, 220, 117 foci (from top to bottom) from 2-3 fields of view from a representative experiment. (**C**) Quantification of mean cytosolic fluorescence for the strains and conditions shown in panel (A). *n* = 50 cells from 2 independent

158 experiments per strain. For (B) and (C), error bars denote standard deviation; */**/***, p<0.05/0.01/0.001 in
159 homoscedastic two-tailed t-tests. The values at pH 7 before and after incubation at pH 4 differ statistically
160 significantly for (B) (***), but not for (C) (p>0.05), except for SctQ (***) and SctL (*). (**D**) Kinetics of EGFP-SctQ
161 dissociation after pH shift from 7 to 4. Overlay of phase contrast (grey) and fluorescence images (yellow); insets,
162 enlarged single bacterium, visualized with the ImageJ red-hot color scale. (**E**) Fluorescence micrographs of Halo-
163 SctL, labeled with JF-646 prior to the first image, during consecutive incubation at different external pH as in
164 (A). Right, overlay of fluorescence distribution at pH prior to and after pH 4 incubation (magenta and green,
165 respectively). Scale bars, 2 µm

166

167 Molecular mechanism of extracellular pH sensing

168 What is the molecular basis for the dissociation of the cytosolic T3SS components at low external pH?
169 To find out whether the pH is sensed intracellularly, we first tested the impact of the changed external
170 pH on the cytosolic pH, using a ratiometric pHluorin GFP variant (pHluorin$_{M153R}$ (Miesenböck et al.,
171 1998; Morimoto et al., 2011)) as a pH sensor. Upon changing the external pH from 7 to 4, the cytosolic
172 pH dropped to a mildly acidic value (pH 6.3-6.4). This cytosolic pH was retained for at least 30 minutes
173 at external pH 4, but quickly recovered upon re-establishment of neutral external pH (Fig. 3A).

174 To test if the observed mild drop in cytosolic pH directly causes the dissociation of the cytosolic
175 complex, we treated bacteria with the proton ionophore 2,4-dinitrophenol, which attunes the
176 cytosolic pH to the external pH (Dechant et al., 2010; Hong et al., 1979; Petrovska et al., 2014) (Suppl.
177 Fig. 7), and visualized the localization of EGFP-SctQ at different pH values. EGFP-SctQ remained
178 localized in foci representing assembled cytosolic complexes at pH 6.3 and below (Fig. 3B), indicating
179 that the observed disassembly of the cytosolic complex is not caused by acidification of the cytosol.

180

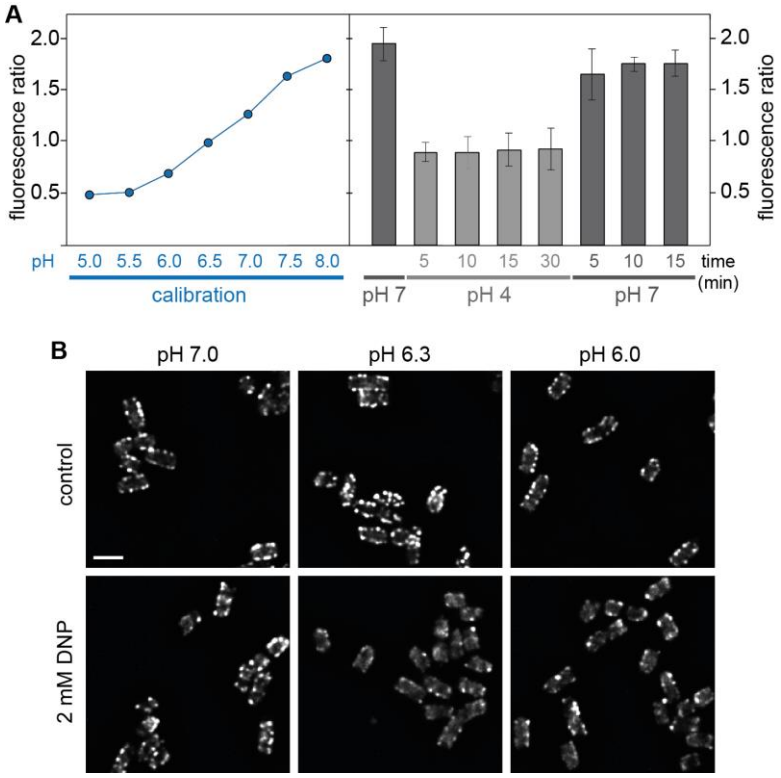

Fig. 3 – Low external pH leads to a small drop in cytosolic pH, which does not induce the dissociation of cytosolic T3SS components

(**A**) Left, calibration of (Ex_{390nm} / Ex_{475nm}) fluorescence ratio of purified $pHluorin_{M153R}$ for the indicated pH values. Technical triplicate, error bars too small to display. Right, determination of cytosolic pH upon changing the external pH from 7 (first column) to 4 (columns 2-5) and back (columns 6-8). Fluorescence ratio (Ex_{390nm} / Ex_{475nm}) of bacteria expressing cytosolic $pHluorin_{M153R}$. *n* = 4, error bars denote standard deviation. (**B**) Fluorescence distribution of EGFP-SctQ in live *Y. enterocolitica* at indicated external pH in absence (top) or presence (bottom) of the ionophore 2,4-dinitrophenol (DNP). Scale bar, 2 µm.

Based on above results, we searched for a periplasmic pH sensor. An obvious candidate is SctD, a bitopic IM protein connecting the outer membrane (OM) ring to the cytosolic components (Fig. 1A) (Hu et al., 2017; Ross and Plano, 2011). Earlier studies showed that lack of SctD, or its inability to bind to SctC, leads to a similar cytosolic location of SctK/L/N/Q as observed at an external pH of 4 (Fig. 2A) (Diepold et al., 2017, 2010), and that the cytosolic domains of SctD connect to SctK via specific interactions (with four SctD binding to one SctK in *Salmonella* SPI-1) (Hu et al., 2017; Tachiyama et al., 2019). This suggests that structural rearrangements of SctD could easily lead to dissociation of SctK and, subsequently, all other cytosolic components.

When we tested the behavior of SctD at low external pH, we found that at pH 4, EGFP-SctD foci in the membrane became less intense than at pH 7, with a concomitant increase in fluorescence throughout the membrane. In contrast to the cytosolic components however, the SctD foci did not completely disappear. Importantly, like the cytosolic components, SctD recovered its localization in foci at neutral external pH (Fig. 4A). To study this unique phenotype in more detail, we performed single-molecule tracking of PAmCherry-SctD proteins in photoactivated localization microscopy (PALM). These

experiments revealed that at an external pH of 7, more than 90% of the SctD molecules in the IM were static; by contrast, at an external pH of 4, more than 40% of the SctD molecules became mobile within the membrane (Fig. 4B, Suppl. Fig. 8), indicating a dissociation from the core injectisome structure at low external pH. Indeed, the large T3SS export apparatus component SctV-EGFP, which diffuses throughout the membrane in the absence of SctD (Diepold et al., 2011), displayed the same behavior at pH 4 compared to pH 7 (Fig. 4C), in line with a release from the SctD structure.

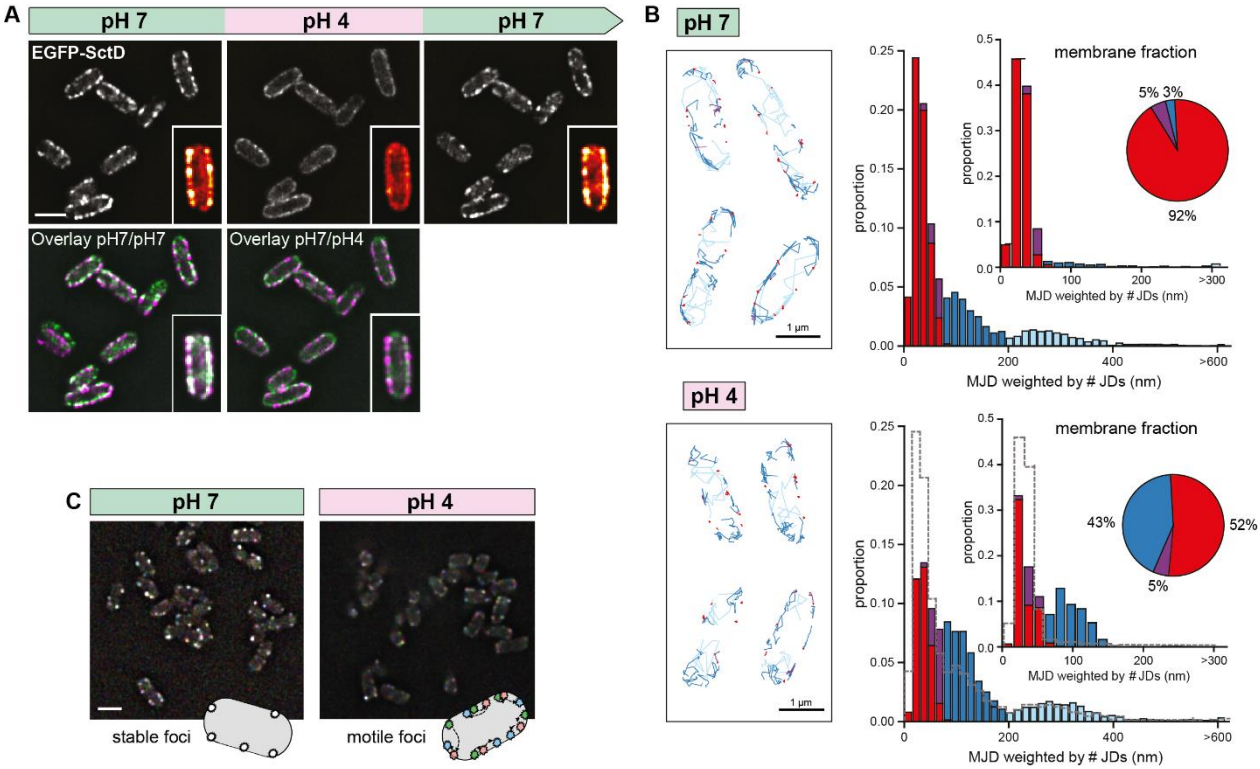

Fig. 4 – The bitopic IM protein SctD senses low external pH

(**A**) Fluorescent micrographs of EGFP-SctD in live *Y. enterocolitica*, consecutively subjected to different external pH in a flow cell. Images were taken under secreting conditions, 10 minutes after bacteria were subjected to the indicated pH. Insets, enlarged single bacteria, visualized with the ImageJ red-hot color scale. Bottom, overlays of fluorescence at pH 7 before pH change (magenta) and pH 7 after pH change or pH 4 (green). (**B**) PAmCherry-SctD dynamics in exemplary living *Y. enterocolitica* (left) and histograms (right) of the mean jump distances (MJD) of PAmCherry-SctD trajectories weighted by the number of jump distances (# JDs) used for calculating each MJD. Only trajectories with more than 6 one-frame jumps are shown and included into the analysis. Upper panel was measured at pH 7, lower panel at pH 4. Trajectories are assigned into two diffusive states: static (red) and mobile (violet and blue fractions) based on the experimental localization precision. The mobile trajectories are sorted into three MJD categories: lower than 60 nm (violet), lower than 195 nm (dark blue) and higher than 195 nm (light blue). Counts are normalized to the total number of trajectories: At pH 7

we acquired 29,859 trajectories (60% static, 2% mobile below 60 nm MJD, 25% mobile from 60 to 195 nm MJD, 13% mobile faster than 195 nm MJD; 19,473 membrane-bound trajectories). At pH 4 we acquired 33,036 trajectories (34% static, 4% mobile below 60 nm MJD, 44% mobile from 60 to 195 nm MJD, 18% mobile faster than 195 nm MJD; 21,600 membrane-bound trajectories). The bin size of 15 nm was calculated using the Freedman-Diaconis rule. The inset histograms display the statistics of only membrane-bound trajectories. Pie plots display the percentage of each MJD category to the total number of membrane-bound trajectories. The number of trajectories of membrane-bound static PAmCherry-SctD molecules decreases in pH 4 (92% to 52%), while the number of diffusing PAmCherry-SctD with MJDs lower than 195 nm (dark blue bars) increases (3% to 43%). The fast fractions of PAmCherry-SctD molecules of MJDs higher than 195 nm (light blue) which are only visible for the whole cell analysis remain constant. The grey dashed lines in the pH 4 panels represent the outlines of the pH 7 analysis. (**C**) Spatial stability of SctV-EGFP foci over time at the indicated external pH. Three images of the same focal plane were taken at 10 s intervals. The green channel shows the cell at t = 0 s, the blue channel at t = 10 s, and the red channel at t = 20 s. Scale bars, 2 µm.

Physiological advantage of temporary suppression of type III secretion at low pH

We reasoned that bacteria could benefit from the dissociation of the cytosolic T3SS components at low external pH to suppress secretion in the stomach, where pH values of 4 and below prevail, which might lead to energy depletion or even elicit immune reactions. If this would indeed be the case, bacteria that do not pass through the stomach during normal infection, and therefore are not under evolutionary pressure to suppress T3SS activity at low pH, might not display the same pH dependence for T3SS activity. We therefore tested the localization of SctQ in *Pseudomonas aeruginosa*. The T3SS of *Y. enterocolitica* and *P. aeruginosa* are closely related evolutionarily (Abby and Rocha, 2012), but the infection strategies of the two species differ. *P. aeruginosa* is not a gastrointestinal pathogen and mainly enters the host body through wounds. SctQ is similar in the two organisms (41% identity, 59% similarity across the complete protein; Suppl. Fig. 9A). In agreement with our hypothesis, the fraction of *P. aeruginosa* cells with EGFP-SctQ foci did not decrease at pH 4 (Fig. 5).

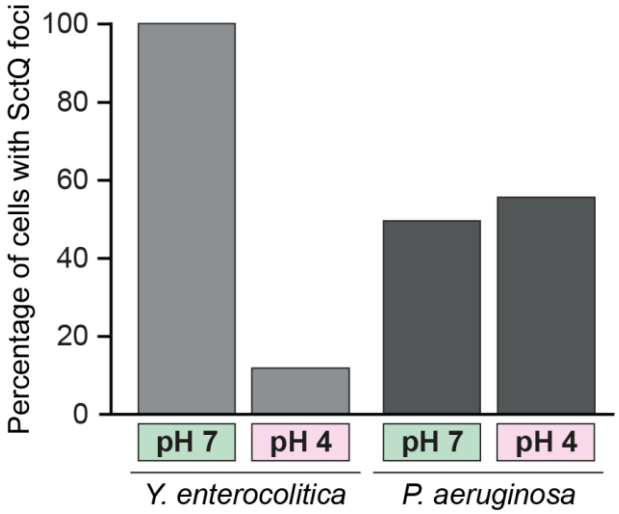

Fig. 5 – The effect of external pH on the assembly of cytosolic T3SS components is species-specific.

Percentage of bacteria with EGFP-SctQ foci at the indicated external pH in *Yersinia enterocolitica* and *Pseudomonas aeruginosa*, respectively. *n* = 246, 472, 155, 182 bacteria from at least 10 fields of view per condition.

To determine a potential molecular mechanism for this effect, we identified amino acids in the periplasmic domain of SctD that could be protonated at pH 4, but not at pH 7 (Asp, Glu, His), and focused on the subset of these amino acids that differ between *Y. enterocolitica* and *P. aeruginosa* (Suppl. Fig. 9B). Single amino acid substitutions, as well as the combination of all four substitutions still led to dissociation of the cytosolic component SctQ, as well as a loss of secretion at pH 4 (Suppl. Fig. 10) suggesting that the effect of the pH might not be conveyed by discrete salt bridges.

After the passage of the stomach, bacteria arrive in the pH-neutral intestine, where they pass the M cells across the intestinal epithelium. At this point, the injectisome must be ready to manipulate immune cells. To test whether the reversible dissociation of the cytosolic T3SS components supports a fast activation of the T3SS once back at neutral pH, we monitored the secretion of effectors over time after a temporary drop of external pH to 4. We found that effector secretion was suppressed at low pH, but recovered within 20-40 minutes after reaching neutral pH (Fig. 6A). Notably, the recovery is much faster than the onset of effector secretion after *de novo* assembly of the T3SS by a temperature change to 37°C (Fig. 6A), supporting the notion that bacteria benefit from the temporary dissociation of the cytosolic subunits at low pH in two ways: This mechanism suppresses protein secretion at low external pH, while ensuring a fast reactivation upon reaching a pH-neutral environment (Fig. 6B).

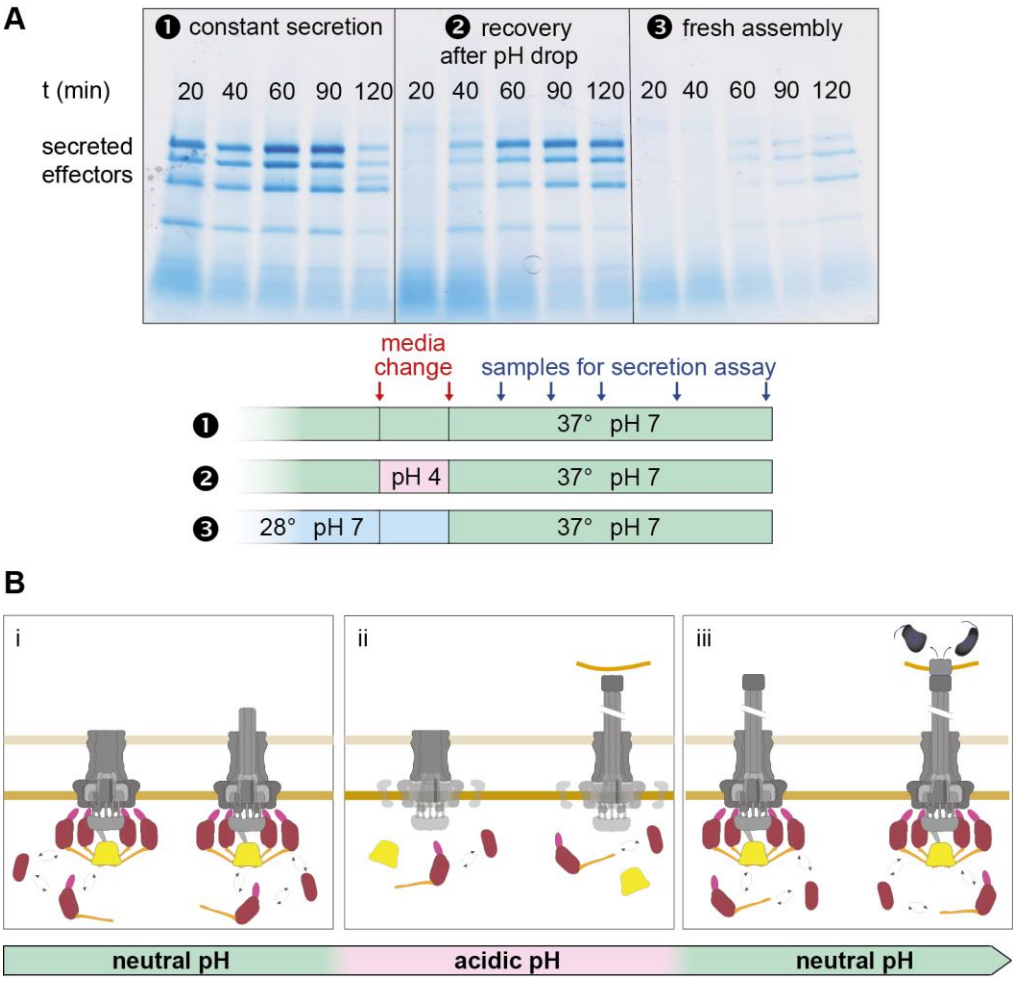

Fig. 6 – Temporary suppression of T3SS activity at low external pH enables a fast re-activation of secretion

(**A**) *In vitro* secretion assay showing the effectors exported by the T3SS at the given time points after the second media change, (1) under constantly secretion-inducing conditions, (2) after a temporary change of the external pH to 4, (3) after incubation at 28°C, where no injectisomes are assembled. (**B**) Model of the pH-dependent suppression of T3SS activity. From left to right: (i) Assembly of the T3SS upon entry into host organisms; cytosolic components bound and exchanging with cytosolic pool. (ii) Continued assembly in the stomach, but no effector translocation upon host cell attachment, because cytosolic components are exclusively cytosolic. (iii) Re-association of cytosolic components to the injectisome and effector translocation upon host cell contact in neutral body parts.

Discussion

On their way through the gastrointestinal system, bacteria encounter a multitude of different pH environments. Importantly, the highly acidic stomach acts as natural barrier for food-borne infections. Gastrointestinal pathogens like *Y. enterocolitica* express factors that facilitate survival in these

conditions, most prominently urease, of which high amounts are exported (Chen et al., 2016; Heroven and Dersch, 2014; Hu et al., 2009; Stingl and De Reuse, 2005; Young et al., 1996). It was not known, however, if and how the activity of the T3SS, an essential virulence factor for many gastrointestinal pathogens, is regulated under these conditions. Although the target cells of the *Y. enterocolitica* T3SS are downstream of the stomach, bacteria can attach to host cells at low pH (Fig. 1B, Suppl. Movies 1-2). Our data support the notion that bacteria prevent premature injection into host cells at this stage by directly using the external pH as a cue for the temporary suppression of the T3SS. While parts of the T3SS, including the needle, remain stable, the cytosolic components dissociate from the injectisome in an acidic environment (pH 4 and below). This effect persists at low external pH; however, once the bacteria encounter neutral external pH, both adherence via the adhesin YadA to collagen is significantly increased (Fig. 1D), and the binding of the cytosolic components is restored (Fig. 2). Bacteria conceivably benefit from this mechanism, which prevents the premature effector translocation into any eukaryotic cells in contact in the acidic regions of the stomach, an event that would be energetically expensive and might elicit immune responses. Secretion can be restored within 20-40 minutes, once the pH-neutral intestine is reached, which is significantly faster than *de novo* synthesis of injectisomes at this time (Fig. 6).

The dissociation kinetics of the cytosolic components of the T3SS revealed a dissociation half-time of about one to two minutes under secreting conditions (Fig. 2D, Suppl. Movie 3). This value is strikingly similar to the exchange rate of SctQ at the injectisome (Diepold et al., 2015), suggesting that at low external pH, primarily the re-association of the cytosolic components is prevented. This adaptation of T3SS function may explain the so-far enigmatic benefit of the observed dynamics of the cytosolic parts of the injectisome during its function. Notably, the observed dissociation of the cytosolic proteins in response to low external pH may not reveal the complete mechanism for suppression of T3SS activity at this pH. The observation that the dissociation of the cytosolic components occurs at a slightly lower pH than the loss of effector secretion, and that the re-initiation of secretion occurs later than the initial recovery of foci indicates that other factors, such as conformational changes in SctD or the cytosolic components might participate in this phenotype. The slightly delayed activation of secretion after restoration of neutral pH could also be explained by the time required for re-associating SctV to the machinery. This delay may, in fact, be beneficial for *Y. enterocolitica*, as it delays the antiphagocytic effects of the T3SS effectors, which otherwise may hamper the passage of *Y.*

enterocolitica through the M cells that is required to access the lymphoid follicles of the Peyer's patches (Cornelis, 2002).

We found that similarly to *E. coli* (Krulwich et al., 2011; Slonczewski et al., 1981), *Y. enterocolitica* can partially compensate for acidic external environment, and that at an external pH of 4.0, the cytosolic pH remained at 6.3-6.4 (Fig. 3A). When we used a proton ionophore to create this cytosolic pH at a similar external pH, the cytosolic T3SS components remained bound to the injectisome (Fig. 3B), suggesting that the external pH is sensed outside the bacterial cytosol. A prime candidate to be involved in external pH sensing is the bitopic IM component SctD, which conceivably senses a drop in external pH with its periplasmic domain and then transmits this signal to the cytosol, either by a direct structural change or by a rearrangement of its interaction within the 24-mer IM ring structure. Both types of pH sensing are used by biological systems: The *E. coli* membrane-integrated transcriptional regulator CadC senses acidic pH through direct protonation of a charged surface patch in its C-terminal periplasmic domain, and transduces the signal to the cytosol by its N-terminal cytosolic domain (Haneburger et al., 2011). Similarly, the *P. syringae* T3SS effector AvrPto transitions from a largely unfolded state in the mildly acidic bacterial cytosol to a well-defined fold in the neutral host cytosol (Dawson et al., 2009). Perhaps most strikingly, the highly ordered multimeric structures of bacteriophages undergo large-scale structural changes at low pH, that are reversible (Helenius et al., 1980; Mauracher et al., 1991; Taylor et al., 2002). Indeed, our data indicate a reversible partial delocalization of SctD at low external pH (Fig. 4). The presence of SctD is required for binding of any cytosolic T3SS component (Diepold et al., 2017, 2010), most likely through a direct contact of four SctD to one SctK at the cytosolic interface of the IM (Hu et al., 2017), indicating that this partial displacement of SctD (Fig. 4) is causal for the dissociation of the cytosolic T3SS components.

Interestingly, SctD is one of the least conserved genes in the T3SS, especially in comparison to its direct structural neighbors, the highly conserved SctC secretin ring in the OM, as well as SctJ and the export apparatus proteins in the IM (Diepold and Wagner, 2014). While this low sequence similarity prevented a multi-sequence alignment to identify conserved differences between the T3SS of gastrointestinal and non-gastrointestinal pathogens (except for the closely related *Y. enterocolitica* and *P. aeruginosa*, Suppl. Fig. 9B), it supports the notion that SctD is involved in species-specific adaptation of the T3SS, such as pH sensing. This hypothesis is further substantiated by the finding that in *P. aeruginosa*, which does not pass the stomach during a normal infection, the effect of low pH is

significantly restricted, with the majority of EGFP-SctQ foci remaining present at low external pH (Fig. 5).

Like the *Y. enterocolitica* T3SS, the intracellular *Salmonella enterica* SPI-2 T3SS is strongly influenced by the external pH; however, the mechanism described for SPI-2 differs from the one described in this study. Injectisome assembly and secretion of the translocon components in SPI-2 are activated by the low pH of the surrounding vacuole (around pH 5.0). After this step, neutral pH, most likely indicative of a successfully established connection to the neutral host cytosol, leads to the disassembly of a gatekeeper complex, which in turn licenses the translocation of effectors (Yu et al., 2010). Strikingly, a single amino acid exchange in the export apparatus protein SctV governs this pH-dependent effect (Yu et al., 2018). Both the sensory and the functional connection between the pH and T3SS activity differ between *Salmonella* SPI-2 and *Y. enterocolitica*, which highlights the high degree of functional adaptability of the T3SS. Taken together, these observations showcase the variety and sophistication of mechanisms that gastrointestinal pathogens have evolved to use different aspects of T3SS assembly and function, including protein dynamics, to tailor the activity of this essential virulence mechanism to their specific needs during infection.

Material and Methods

Bacterial strain generation and genetic constructs

A list of strains and plasmids used in this study can be found in Supplementary Table 1. The strains used in this study are based on the *Y. enterocolitica* wild-type strain MRS40 (Sory et al., 1995), and the strain IML421asd (ΔHOPEMTasd), in which all major virulence effector proteins (YopH,O,P,E,M,T) are deleted (Kudryashev et al., 2013). Furthermore, this strain harbors a deletion of the aspartate-beta-semialdehyde dehydrogenase gene which render the strain auxotrophic for diaminopimelic acid (DAP).

All fusion proteins used were expressed as endogenous fusions from their native location on the pYV virulence plasmid, which were introduced by two step homologous recombination (Kaniga et al., 1991).

For cloning and conjugation the *E. coli* strains Top10 and SM10 λpir were used, respectively. All constructs were confirmed by sequencing (Eurofins Scientific). Constructs with single amino acid

substitutions in SctD were created by overlapping PCR using Phusion polymerase (New England Biolabs), and expressed from an arabinose controlled expression vector (pBAD). Expression was induced by addition of 0.2-0.4% arabinose (as indicated) at the time of the induction of T3SS expression (temperature increase to 37°C).

Bacterial cultivation, in vitro secretion assays and fluorescence microscopy

Y. enterocolitica day cultures were inoculated from stationary overnight cultures to an OD_{600} of 0.15 and 0.12 for secreting and non-secreting conditions, respectively, in BHI medium (Suppl. Table 2) supplemented with nalidixic acid (35 mg/ml), diaminopimelic acid (80 mg/ml), where required, glycerol (0.4%) and $MgCl_2$ (20 mM). Where required, ampicillin was added (0.2 mg/ml) to select for pBAD-based plasmids. For secreting conditions, cultures were additionally supplemented with 5 mM EGTA; for non-secreting conditions, cultures were additionally supplemented with 5 mM $CaCl_2$ and filtered through a 0.45 µm filter. Cultures were incubated at 28°C for 90 minutes. At this time point, expression of the *yop* regulon was induced by a rapid temperature shift to 37°C in a water bath for 2-3 h. At the temperature upshifts, pBAD-based genes were induced by addition of 0.2-0.4% arabinose (as indicated).

For effector visualization or total cell analysis, the cells were incubated at 37°C between 1-3 hours, as described. Then, 2 ml of the culture were collected at 21,000 *g* for 10 min. The supernatant was separated from the cell fraction and precipitated with trichloroacetic acid (TCA) for 1-8 h at 4°C. Proteins were collected by centrifugation for 20 min at 21,000 *g* and 4°C, washed once with ice cold acetone and then resuspended and normalized in SDS-PAGE loading buffer. Total cell samples were normalized to $2.5x10^8$ bacteria in SDS loading. Afterwards the samples were incubated for 5 minutes at 99°C and loaded on 12-20% SDS-PAGE gels and stained after running with Instant blue (Expedeon).

For fluorescence microscopy, bacteria were grown at 37°C. After 2-3 h, 400 µl of bacterial culture were collected by centrifugation (2,400 *g*, 2 min) and resuspended in 200µl microscopy minimal medium (Suppl. Table 2). Cells were spotted on glass depression slides on 1.5% low melting agarose pads (Sigma) in microscopy minimal medium. Where required, 80 mg/ml DAP for ΔHOPEMTasd-based strains, 0.2-0.4% L-arabinose for induction of *in trans* expression, 5 mM Ca^{2+} for non-secreting conditions, or 5 mM EGTA for secreting conditions were added.

*P. aeruginosa o*vernight cultures were grown at 28°C. For secreting cultures, LB broth (Suppl. Table 2) was supplemented with 20 mM $MgCl_2$, 200mM NaCl and 5 mM EGTA and inoculated to an OD_{600} of

0.15 and incubated for 2 h at 37°C. This culture was then used to inoculate a fresh culture containing the same supplements to an OD_{600} of 0.15. Microscopy experiments were then performed 2 h later on a minimal media agar pad and in LB medium.

Wide field fluorescence microscopy

Microscopy was performed on a Deltavision Elite Spectris Optical Sectioning Microscope (Applied Precision), equipped with a UApo N 100x/1.49 oil TIRF UIS2 objective (Olympus), using an Evolve EMCCD Camera (Photometrics). The sample was illuminated for 0.1 s with a 488laser with a TIRF depth setting of 3440. The micrographs where then deconvolved using softWoRx 7.0.0 (standard "conservative" settings). Images were then further processed for presentation with ImageJ-Fiji. Where necessary, drift correction was performed with the StackReg Plugin. A representative field of view was selected, brightness and contrast of the micrographs was adjusted to the same level and false colors selected.

Samples sizes and number of replicates for wide field microscopy and all other experiments were determined prior to the experiments, based on experimental feasibility and their potential to draw clear conclusions. These numbers were not changed based on the experimental outcome.

Flow cell based TIRF microscopy

A microscopy flow cell was manufactured based on (Berg and Block, 1984). Formation of injectisomes was induced under non-secreting conditions. After formation of the injectisomes, bacteria were collected and resuspended in approximately 0.5 volumes of microscopy medium supplemented with 80 mg/ml DAP and 5mM EGTA. The flow cell was pre-incubated with microscopy medium and the bottom coverslip (25 mm No. 1.5; VWR) was attached to the cell. Bacteria were spotted on a coverslip and incubated on the coverslip for 1 min to insure attachment to the glass surface. In a next step the flow cell was flooded with 60 µl of minimal media and sealed from the top with an additional cover slip. The flow cell was mounted on the microscopy stage and buffer flow in the chamber by gravity-driven flow was induced using a 1 ml syringe. To exchange the buffers in the flow cell, the tube was quickly relocated to the new buffer. Complete buffer exchange in the flow cell was determined to take 39 ± 5 s ($n = 7$).

Detection and quantification of fluorescent foci

Quantitative foci detection was performed by first segmenting the images using the software BiofilmQ. After segmentation, we extended the functionality of the fluorescence property calculations within BiofilmQ, by detecting the characteristics of fluorescence foci. The foci were filtered by their intensity above the background intensity of the cell, calculated by subtracting a blurred image.

Maleimide based needle staining

To visualize the injectisome needles, expression of $SctF_{S5C}$ (Milne-Davies et al., 2019) was induced from plasmid. Protein expression was induced with 0.4% L-arabinose at the temperature shift. After 2-3 h, bacteria were collected and resuspended in 0.2 volumes of microscopy medium supplemented with 5 µM of a CF^{TM}488A/633 maleimide dye (Sigma-Aldrich, USA) for 5 min in 100 µl of minimal media at 37°C. After staining, cells were washed once with 500µl of minimal medium and spotted on 1.5% agarose pads in the same medium.

Halo staining with Janelia fluorescent dyes

To stain and visualize a defined pool of T3SS proteins, Halo-labeled proteins were visualized using Janelia Fluor 549-NHS ester and Janelia Fluor 646-NHS ester. 500 µl of bacterial culture were collected by centrifugation (2,400 *g*, 2 min) and resuspended in 100 µl microscopy medium. Bacteria were stained with 0.2 µM Janelia Fluor JF-646/JF-549 dyes for 37°C for 30 min in a tabletop shaker. Afterwards, bacteria were washed twice in 500 µl minimal medium and then mounted on the flow cell or 1.5% agarose pads in the same medium.

Equilibration of cytosolic and external pH

2,4-dinitrophenol (DNP) was diluted in methanol and used in a final concentration of 2 mM in microscopy minimal media. Cells were grown under the conditions described above, and resuspended in DNP containing media immediately before being spotted on 1.5% agarose pads in the same medium.

Bacterial survival test

Wild-type MRS40 *Y. enterocolitica* were inoculated to an OD_{600} of 0.12 in non-secreting conditions and incubated for 1.5 h at 28°C to reach exponential growth phase. Then cells were collected by centrifugation at 2,400 *g* for 2 min. The supernatant was discarded and the pellets were resuspended in a range of pH-adjusted media buffered with 50 mM glycine, 50 mM HEPES and 50 mM MES. These cultures were incubated for 15 min at 28°C and afterwards a dilution series in neutral media was

performed. For the visualization, 4 µl of bacterial suspension were spotted on a neutral LB agar supplemented with nalidixic acid and incubated at 28°C overnight.

pHluorin purification and calibration

For purification, the protocol described by Nakamura et al. (Nakamura et al., 2009) was adapted for bench top purification. Expression of ratiometric GST-pHluorin$_{M153R}$ in *E. coli* DH5αZI was induced in a 500 ml culture with 1 mM IPTG, followed by 4 h incubated at 28°C. Cells were harvested and stored for further processing at -80°C. Next, cells were thawed on ice, resuspended in lysis buffer and disrupted by two passages through a French Press. The lysate was centrifuged (25,000 rpm, 60 min, 4°C) and then mixed with the previously equilibrated glutathione agarose and gently mixed at 4°C for 1.5 h in a small spinning wheel. The agarose was collected by centrifugation (500 *g*, 5 min) and washed 3 times with PBS. Thrombin digest was performed in 2 ml PBS while incubating for 60 min on a roll mill. Agarose was removed by centrifugation (500 *g*, 5 min) and the protein was stored at -80°C for further use.

The calibration was performed on a Deltavision Elite microscope. 5 µl of purified pHluorin protein was spotted on a KOH-cleaned microscopy slide in an enclosed compartment (Thermo Fisher Scientific GeneFrame, AB-0577) and incubated for 5 min to ensure attachment to the glass surface. Then, 10 µl of pH-adjusted PBS buffered with 200 mM glycine, 200 mM HEPES, and 200 mM MES were added. Ratiometric pHluorin fluorescence was determined using the DAPI excitation filter (390/18nm) or GFP excitation filter (475/28nm) at 32% illumination intensity, in combination with a GFP emission filter set (525/48nm) with 0.3 s exposure time. The overall fluorescence of the images before deconvolution were determined and corrected for background, which was measured with an empty slide filled with PBS. The ratio of DAPI/Green vs Green/Green fluorescence was determined for a pH range from pH 8 – pH 5 in 0.5 pH steps.

Single particle tracking photoactivated localization microscopy (sptPALM)

Bacteria were cultivated under non-secreting conditions as described above. After 2.5 h of incubation at 37°C, the media was changed to pre warmed (37°C) minimal microscopy medium containing the same supplements as the BHI before. Cells were incubated for 30 min and then washed four times in 5 volumes of pre-warmed (37°C) EZ medium (Supplementary Table 2) supplemented with DAP and 5 mM $CaCl_2$. Bacteria were concentrated 2x after the last wash and spotted on a 1.5% agarose pad in EZ medium supplemented with DAP and 5 mM $CaCl_2$ on a KOH-cleaned microscopy slide in an

enclosed compartment (Thermo Fisher Scientific GeneFrame, AB-0577). Imaging was performed on a custom build setup based on an automated Nikon Ti Eclipse microscope equipped with appropriate dichroic and filters (ET DAPI/FITC/Cy3 dichroic, ZT405/488/561rpc rejection filter, ET610/75 bandpass, Chroma), and a CFI Apo TIRF 100x oil objective (NA 1.49, Nikon). All lasers (405 nm OBIS, 561 nm OBIS; all Coherent Inc. USA) were modulated via an acousto-optical tunable filter (AOTF) (Gooch and Housego, USA). Fluorescence was detected by an EMCCD camera (iXON Ultra 888, Andor, UK) in frame transfer mode and read-out parameter settings of EM-gain 300, pre-amp gain 2 and 30 MHz read-out speed. The z-focus was controlled using a commercial perfect focus system (Nikon). Acquisitions were controlled by a customized version of Micro-Manager (Edelstein et al., 2010). Live cell sptPALM experiments were performed on a customized heating stage at 25°C. Live *Y. enterocolitica* PAmCherry-SctD cells were imaged in HILO illumination mode (Tokunaga et al., 2008). Applied laser intensities measured after objective were 35 W/cm^2 (405 nm) and 800 W/cm^2 (561 nm). Prior to recording each new region of interest (ROI), a pre-bleaching step of 561 nm illumination was applied for 30 seconds to reduce autofluorescence. Movies were then recorded for 2000 frames pulsing the 405 nm laser every 20th imaging frame at 5 Hz with an exposure time of 200 ms per frame. After sptPALM imaging, a bright light snapshot of all illuminated regions was recorded to obtain the bacterial cell shapes.

Single molecule localizations were obtained using *rapidSTORM* 3.3.1 (Wolter et al., 2012) and single cells were manually segmented in *Fiji (ImageJ 1.51f)* (Schindelin et al., 2012). sptPALM data was tracked, visualized and filtered using a customized tracking software written in C++ (***swift***, unpublished software, RG Endesfelder). Trajectories were allowed to have a maximum of 5 frames of gap time (e.g. caused by fluorophore blinking). Trajectories were assigned to their diffusive states (static and mobile) on the basis of the experimental localization precision of about 25 nm (determined by the NeNA method (Endesfelder et al., 2014). For trajectories with more than 6 one-frame jumps, the mean jump distance (MJD) was calculated (jumps spanning several frames due to dark times were not used in MJD calculations). The obtained MJDs were weighted by the number of jumps and displayed in a histogram using OriginPro 9.4 (Origin LAB Corporation, USA).

Y. enterocolitica YadA and cellular adhesion assays

To measure YadA adhesion to collagen at different pH values, an ELISA-like binding assay was performed (Leo et al., 2010, 2008; Saragliadis and Linke, 2019). Clear 96 well plates (Sarstedt, Ref. 82.1581) were coated with 100 µl of calf collagen type I (10 µg/ml, ThermoFisher A1064401) in H_2O

with 0.01 M acetic acid for 1h at room temperature (RT). The supernatant was discarded and the wells were blocked with 1% BSA in PBS and afterwards washed three times with 0.1% BSA in PBS. Afterwards, 100 µL of purified YadA head domains with a C-terminal His_6-tag at a concentration of 10 µg/mL were incubated in the wells. In order to test binding at different pH, the YadA heads were diluted in acetic acid/sodium acetate at pH 4.0 or pH 5.0 and for higher pH values in PBS at pH 6.0 and 7.0. Binding was allowed for 1 h at RT. Afterwards, the plate was emptied and washed three times with 0.1% BSA in PBS. The wells were blocked with 1.0% BSA in PBS for 1h at RT. For detection, Ni-HRP conjugates (HisProbe-HRP, Thermo Fisher Scientific, Ref. 15165) were diluted in 0.1% BSA in PBS and 100 µl per well were incubated for 1 h at RT. The Ni-HRP conjugate solution was discarded and the wells washed three times with PBS. Detection was performed using ABTS substrate (Thermo Scientific. Ref. 34026). Development was allowed for 30 min. Absorption was measured at 405 nm on a plate reader (Biotek Synergy H1).

Glass binding assays for live *Y. enterocolitica* were performed in a flow cell. Bacteria were treated as mentioned above, resuspended in microscopy medium at the indicated pH value, and added to the flow cell as described above. Bacteria were tracked visually for 10 min afterwards.

Acknowledgements

We thank Marc Erhardt (Humboldt University Berlin, Germany), Tohru Minamino (Osaka University, Japan), and Gero Miesenböck (University of Oxford, UK) for the $pHluorin_{M153R}$ DNA, and Luke Lavis (Janelia Research Campus, USA) for the kind gift of Janelia Fluor dyes.

This work was supported by the Max Planck Society. It was also funded by the Horizon 2020 Innovative Training Network “ViBrANT” (to DL).

References

Abby SS, Rocha EPC. 2012. The non-flagellar type III secretion system evolved from the bacterial flagellum and diversified into host-cell adapted systems. *PLoS Genet* **8**:e1002983. doi:10.1371/journal.pgen.1002983

Berg HC, Block SM. 1984. A Miniature Flow Cell Designed for Rapid Exchange of Media Under High-power Microscope Objectives. *Microbiology* **130**:2915–2920. doi:10.1099/00221287-130-11-2915

Bernal I, Börnicke J, Heidemann J, Svergun D, Horstmann JA, Erhardt M, Tuukkanen A, Uetrecht C, Kolbe M. 2019. Molecular Organization of Soluble Type III Secretion System Sorting Platform Complexes. *J Mol Biol* **431**:3787–3803. doi:10.1016/j.jmb.2019.07.004

574 Büttner D. 2012. Protein export according to schedule: architecture, assembly, and regulation of type
575 III secretion systems from plant- and animal-pathogenic bacteria. *Microbiol Mol Biol Rev* **76**:262–
576 310. doi:10.1128/MMBR.05017-11

577 Chen S, Thompson KM, Francis MS. 2016. Environmental Regulation of Yersinia Pathophysiology.
578 *Front Cell Infect Microbiol* **6**:25. doi:10.3389/fcimb.2016.00025

579 Clerc P, Baudry B, Sansonetti PJ. 1986. Plasmid-mediated contact haemolytic activity in Shigella
580 species: correlation with penetration into HeLa cells. *Ann Inst Pasteur Microbiol* **137A**:267–78.

581 Coburn B, Sekirov I, Finlay BB. 2007. Type III secretion systems and disease. *Clin Microbiol Rev* **20**:535–
582 49. doi:10.1128/CMR.00013-07

583 Cornelis GR. 2006. The type III secretion injectisome. *Nat Rev Microbiol* **4**:811–825.
584 doi:10.1038/nrmicro1526

585 Cornelis GR. 2002. Yersinia type III secretion: Send in the effectors. *J Cell Biol* **158**:401–408.
586 doi:10.1083/jcb.200205077

587 Dawson JE, Seckute J, De S, Schueler SA, Oswald AB, Nicholson LK. 2009. Elucidation of a pH-folding
588 switch in the Pseudomonas syringae effector protein AvrPto. *Proc Natl Acad Sci U S A* **106**:8543–8.
589 doi:10.1073/pnas.0809138106

590 Dechant R, Binda M, Lee SS, Pelet S, Winderickx J, Peter M. 2010. Cytosolic pH is a second messenger
591 for glucose and regulates the PKA pathway through V-ATPase. *EMBO J* **29**:2515–26.
592 doi:10.1038/emboj.2010.138

593 Diepold A, Amstutz M, Abel S, Sorg I, Jenal U, Cornelis GR. 2010. Deciphering the assembly of the
594 Yersinia type III secretion injectisome. *EMBO J* **29**:1928–1940. doi:10.1038/emboj.2010.84

595 Diepold A, Kudryashev M, Delalez NJ, Berry RM, Armitage JP. 2015. Composition, Formation, and
596 Regulation of the Cytosolic C-ring, a Dynamic Component of the Type III Secretion Injectisome.
597 *PLOS Biol* **13**:e1002039. doi:10.1371/journal.pbio.1002039

598 Diepold A, Sezgin E, Huseyin M, Mortimer T, Eggeling C, Armitage JP. 2017. A dynamic and adaptive
599 network of cytosolic interactions governs protein export by the T3SS injectisome. *Nat Commun*
600 **8**:15940. doi:10.1038/ncomms15940

601 Diepold A, Wagner S. 2014. Assembly of the bacterial type III secretion machinery. *FEMS Microbiol*
602 *Rev* **38**:802–22. doi:10.1111/1574-6976.12061

603 Diepold A, Wiesand U, Cornelis GR. 2011. The assembly of the export apparatus (YscR,S,T,U,V) of the
604 Yersinia type III secretion apparatus occurs independently of other structural components and
605 involves the formation of an YscV oligomer. *Mol Microbiol* **82**:502–14. doi:10.1111/j.1365-
606 2958.2011.07830.x

607 Edelstein A, Amodaj N, Hoover K, Vale R, Stuurman N. 2010. Computer control of microscopes using
608 μManager. *Curr Protoc Mol Biol* **Chapter 14**:Unit14.20. doi:10.1002/0471142727.mb1420s92

609 Endesfelder U, Malkusch S, Fricke F, Heilemann M. 2014. A simple method to estimate the average
610 localization precision of a single-molecule localization microscopy experiment. *Histochem Cell Biol*
611 **141**:629–38. doi:10.1007/s00418-014-1192-3

612 Evans DF, Pye G, Bramley R, Clark AG, Dyson TJ, Hardcastle JD. 1988. Measurement of gastrointestinal
613 pH profiles in normal ambulant human subjects. *Gut* **29**:1035–41. doi:10.1136/gut.29.8.1035

614 Grimm JB, Brown TA, English BP, Lionnet T, Lavis LD. 2017. Synthesis of Janelia Fluor HaloTag and

SNAP-Tag Ligands and Their Use in Cellular Imaging Experiments. *Methods Mol Biol* **1663**:179–188. doi:10.1007/978-1-4939-7265-4_15

Håkansson S, Schesser K, Persson C, Galyov EE, Rosqvist R, Homblé F, Wolf-Watz H. 1996. The YopB protein of Yersinia pseudotuberculosis is essential for the translocation of Yop effector proteins across the target cell plasma membrane and displays a contact-dependent membrane disrupting activity. *EMBO J* **15**:5812–5823.

Haneburger I, Eichinger A, Skerra A, Jung K. 2011. New insights into the signaling mechanism of the pH-responsive, membrane-integrated transcriptional activator CadC of Escherichia coli. *J Biol Chem* **286**:10681–9. doi:10.1074/jbc.M110.196923

Helenius A, Kartenbeck J, Simons K, Fries E. 1980. On the entry of Semliki forest virus into BHK-21 cells. *J Cell Biol* **84**:404–20. doi:10.1083/jcb.84.2.404

Heroven AK, Dersch P. 2014. Coregulation of host-adapted metabolism and virulence by pathogenic yersiniae. *Front Cell Infect Microbiol* **4**:146. doi:10.3389/fcimb.2014.00146

Hong JS, Hunt AG, Masters PS, Lieberman MA. 1979. Requirements of acetyl phosphate for the binding protein-dependent transport systems in Escherichia coli. *Proc Natl Acad Sci U S A* **76**:1213–7. doi:10.1073/pnas.76.3.1213

Hu B, Lara-Tejero M, Kong Q, Galán JE, Liu J. 2017. In Situ Molecular Architecture of the Salmonella Type III Secretion Machine. *Cell* **168**:1065–1074.e10. doi:10.1016/j.cell.2017.02.022

Hu B, Morado DR, Margolin W, Rohde JR, Arizmendi O, Picking WL, Picking WD, Liu J. 2015. Visualization of the type III secretion sorting platform of Shigella flexneri. *Proc Natl Acad Sci* **112**:1047–1052. doi:10.1073/pnas.1411610112

Hu Y, Lu P, Wang Y, Ding L, Atkinson S, Chen S. 2009. OmpR positively regulates urease expression to enhance acid survival of Yersinia pseudotuberculosis. *Microbiology* **155**:2522–2531. doi:10.1099/mic.0.028381-0

Hueck CJ. 1998. Type III protein secretion systems in bacterial pathogens of animals and plants. *Microbiol Mol Biol Rev* **62**:379–433.

Jackson MW, Plano G V. 2000. Interactions between type III secretion apparatus components from Yersinia pestis detected using the yeast two-hybrid system. *FEMS Microbiol Lett* **186**:85–90.

Kaniga K, Delor I, Cornelis GR. 1991. A wide-host-range suicide vector for improving reverse genetics in Gram-negative bacteria: inactivation of the blaA gene of Yersinia enterocolitica. *Gene* **109**:137–141. doi:10.1016/0378-1119(91)90599-7

Keller B, Mühlenkamp M, Deuschle E, Siegfried A, Mössner S, Schade J, Griesinger T, Katava N, Braunsdorf C, Fehrenbacher B, Jiménez-Soto LF, Schaller M, Haas R, Genth H, Retta SF, Meyer H, Böttcher RT, Zent R, Schütz M, Autenrieth IB, Bohn E. 2015. Yersinia enterocolitica exploits different pathways to accomplish adhesion and toxin injection into host cells. *Cell Microbiol* **17**:1179–1204. doi:10.1111/cmi.12429

Krulwich TA, Sachs G, Padan E. 2011. Molecular aspects of bacterial pH sensing and homeostasis. *Nat Rev Microbiol* **9**:330–343. doi:10.1038/nrmicro2549

Kudryashev M, Stenta M, Schmelz S, Amstutz M, Wiesand U, Castaño-Díez D, Degiacomi MTM, Münnich S, Bleck CKC, Kowal J, Diepold A, Heinz DWD, Dal Peraro M, Cornelis GR, Stahlberg H. 2013. In situ structural analysis of the Yersinia enterocolitica injectisome. *Elife* **2**:e00792. doi:10.7554/eLife.00792

Lara-Tejero M, Kato J, Wagner S, Liu X, Galán JE. 2011. A Sorting Platform Determines the Order of Protein Secretion in Bacterial Type III Systems. *Science (80-)* **331**:1188–91. doi:10.1126/science.1201476

Leo JC, Elovaara H, Bihan D, Pugh N, Kilpinen SK, Raynal N, Skurnik M, Farndale RW, Goldman A. 2010. First analysis of a bacterial collagen-binding protein with collagen toolkits: Promiscuous binding of YadA to collagens may explain how YadA interferes with host processes. *Infect Immun* **78**:3226–3236. doi:10.1128/IAI.01057-09

Leo JC, Elovaara H, Brodsky B, Skurnik M, Goldman A. 2008. The Yersinia adhesin YadA binds to a collagenous triple-helical conformation but without sequence specificity. *Protein Eng Des Sel* **21**:475–484. doi:10.1093/protein/gzn025

Leo JC, Oberhettinger P, Schütz M, Linke D. 2015. The inverse autotransporter family: intimin, invasin and related proteins. *Int J Med Microbiol* **305**:276–82. doi:10.1016/j.ijmm.2014.12.011

Mauracher CA, Gillam S, Shukin R, Tingle AJ. 1991. pH-dependent solubility shift of rubella virus capsid protein. *Virology* **181**:773–777. doi:10.1016/0042-6822(91)90916-Y

McClements DJ, Li Y. 2010. Review of in vitro digestion models for rapid screening of emulsion-based systems. *Food Funct* **1**:32. doi:10.1039/c0fo00111b

Meuskens I, Saragliadis A, Leo JCC, Linke D. 2019. Type V Secretion Systems: An Overview of Passenger Domain Functions. *Front Microbiol* **10**:1–19. doi:10.3389/fmicb.2019.01163

Miesenböck G, De Angelis DA, Rothman JE. 1998. Visualizing secretion and synaptic transmission with pH-sensitive green fluorescent proteins. *Nature* **394**:192–5. doi:10.1038/28190

Milne-Davies B, Helbig C, Wimmi S, Cheng DWC, Paczia N, Diepold A. 2019. Life After Secretion—Yersinia enterocolitica Rapidly Toggles Effector Secretion and Can Resume Cell Division in Response to Changing External Conditions. *Front Microbiol* **10**:2128. doi:10.3389/fmicb.2019.02128

Morimoto Y V, Kojima S, Namba K, Minamino T. 2011. M153r mutation in a ph-sensitive green fluorescent protein stabilizes its fusion proteins. *PLoS One* **6**:e19598. doi:10.1371/journal.pone.0019598

Mota LJ, Journet L, Sorg I, Agrain C, Cornelis GR. 2005. Bacterial injectisomes: needle length does matter. *Science (80-)* **307**:2005.

Mühlenkamp M, Oberhettinger P, Leo JC, Linke D, Schütz MS. 2015a. Yersinia adhesin A (YadA)--beauty & beast. *Int J Med Microbiol* **305**:252–8. doi:10.1016/j.ijmm.2014.12.008

Mühlenkamp M, Oberhettinger P, Leo JCC, Linke D, Schütz MSS. 2015b. Yersinia adhesin A (YadA) - Beauty & beast. *Int J Med Microbiol* **305**:252–258. doi:10.1016/j.ijmm.2014.12.008

Nakamura S, Kami-ike N, Yokota JP, Kudo S, Minamino T, Namba K. 2009. Effect of Intracellular pH on the Torque?Speed Relationship of Bacterial Proton-Driven Flagellar Motor. *J Mol Biol* **386**:332–338. doi:10.1016/j.jmb.2008.12.034

Nans A, Kudryashev M, Saibil HR, Hayward RD. 2015. Structure of a bacterial type III secretion system in contact with a host membrane in situ. *Nat Commun* **6**:10114. doi:10.1038/ncomms10114

Petrovska I, Nüske E, Munder MC, Kulasegaran G, Malinovska L, Kroschwald S, Richter D, Fahmy K, Gibson K, Verbavatz J-M, Alberti S. 2014. Filament formation by metabolic enzymes is a specific adaptation to an advanced state of cellular starvation. *Elife* **3**. doi:10.7554/eLife.02409

Rocha JM, Richardson CJ, Zhang M, Darch CM, Cai E, Diepold A, Gahlmann A. 2018. Single-molecule

tracking in live Yersinia enterocolitica reveals distinct cytosolic complexes of injectisome subunits. *Integr Biol* **10**:502–515. doi:10.1039/C8IB00075A

Ross J, Plano G V. 2011. A C-Terminal Region of Yersinia pestis YscD Binds the Outer Membrane Secretin YscC. *J Bacteriol* **193**:2276–2289.

Saragliadis A, Linke D. 2019. Assay development for the discovery of small-molecule inhibitors of YadA adhesion to collagen. *Cell Surf* **5**:100025. doi:10.1016/j.tcsw.2019.100025

Schindelin J, Arganda-Carreras I, Frise E, Kaynig V, Longair M, Pietzsch T, Preibisch S, Rueden C, Saalfeld S, Schmid B, Tinevez J-Y, White DJ, Hartenstein V, Eliceiri K, Tomancak P, Cardona A. 2012. Fiji: an open-source platform for biological-image analysis. *Nat Methods* **9**:676–682. doi:10.1038/nmeth.2019

Slonczewski JL, Rosen BP, Alger JR, Macnab RM. 1981. pH homeostasis in Escherichia coli: measurement by 31P nuclear magnetic resonance of methylphosphonate and phosphate. *Proc Natl Acad Sci U S A* **78**:6271–5.

Sory M-P, Boland A, Lambermont I, Cornelis GR. 1995. Identification of the YopE and YopH domains required for secretion and internalization into the cytosol of macrophages, using the cyaA gene fusion approach. *Proc Natl Acad Sci U S A* **92**:11998–12002.

Stingl K, De Reuse H. 2005. Staying alive overdosed: How does Helicobacter pylori control urease activity? *Int J Med Microbiol* **295**:307–315. doi:10.1016/J.IJMM.2005.06.006

Tachiyama S, Chang Y, Muthuramalingam M, Hu B, Barta ML, Picking WL, Liu J, Picking WD. 2019. The cytoplasmic domain of MxiG interacts with MxiK and directs assembly of the sorting platform in the Shigella type III secretion system. *J Biol Chem* jbc.RA119.009125. doi:10.1074/jbc.RA119.009125

Taylor DJ, Krishna NK, Canady MA, Schneemann A, Johnson JE. 2002. Large-scale, pH-dependent, quaternary structure changes in an RNA virus capsid are reversible in the absence of subunit autoproteolysis. *J Virol* **76**:9972–80. doi:10.1128/jvi.76.19.9972-9980.2002

Tertti R, Skurnik M, Vartio T, Kuusela P. 1992. Adhesion protein YadA of Yersinia species mediates binding of bacteria to fibronectin. *Infect Immun* **60**:3021–3024.

Tokunaga M, Imamoto N, Sakata-Sogawa K. 2008. Highly inclined thin illumination enables clear single-molecule imaging in cells. *Nat Methods* **5**:159–61. doi:10.1038/nmeth1171

Wolter S, Löschberger A, Holm T, Aufmkolk S, Dabauvalle M-C, van de Linde S, Sauer M. 2012. rapidSTORM: accurate, fast open-source software for localization microscopy. *Nat Methods* **9**:1040–1. doi:10.1038/nmeth.2224

Young GM, Amid D, Miller VL. 1996. A bifunctional urease enhances survival of pathogenic Yersinia enterocolitica and Morganella morganii at low pH. *J Bacteriol* **178**:6487–95. doi:10.1128/JB.178.22.6487-6495.1996

Yu X-J, Grabe GJ, Liu M, Mota LJ, Holden DW. 2018. SsaV Interacts with SsaL to Control the Translocon-to-Effector Switch in the Salmonella SPI-2 Type Three Secretion System. *MBio* **9**:e01149-18. doi:10.1128/mBio.01149-18

Yu X-J, McGourty K, Liu M, Unsworth KE, Holden DW. 2010. pH sensing by intracellular Salmonella induces effector translocation. *Science (80-)* **328**:1040–3. doi:10.1126/science.1189000

Strain	**Genotype**	**Reference**
MRS40	Wild-type pYV *Y. enterocolitica* E40 *ΔblaA*	(Sory et al., 1995)
IML421*asd* (HOPEMTasd)	MRS40 $yopO_{\Delta 12\text{-}427}$ $yopE_{21}$ $yopH_{\Delta 11\text{-}352}$ $yopM_{23}$ $yopP_{23}$ $yopT_{135}$ *Δasd*	(Kudryashev et al., 2013)
AD4016	MRS40 *egfp-sctQ*	(Diepold et al., 2010)
AD4085	IML421*asd egfp-sctQ*	(Kudryashev et al., 2013)
AD4175	IML421*asd sctV-egfp* (mutated with pAD208)	This work
AD4306	IML421*asd egfp-sctD*	(Diepold et al., 2015)
AD4411	IML421*asd egfp-sctQ ΔsctD*	(Diepold et al., 2017)
AD4439	IML421*asd pamcherry1-sctD* (mutated with pAD439)	This work
AD4474	IML421*asd efgp-sctK*	(Diepold et al., 2017)
ADTM4514	IML421*asd egfp-sctN*	(Diepold et al., 2017)
ADTM4520	IML421*asd egfp-sctL*	(Diepold et al., 2017)
ADTM4521	IML421*asd mcherry-sctL*	(Diepold et al., 2017)
ADTM4525	IML421*asd halo-sctL*	(Diepold et al., 2017)
ADMH4536	IML421*asd halo-sctL ΔsctF*	This work
DL001	*P. aeruginosa* PAO1 *egfp-sctQ*	Lampaki *et al*., 2019 (submitted)

Plasmids	**Genotype**	**Reference**
pBAD-His B	pBR322-derived expression vector	Invitrogen
pKNG101	*oriR6K sacBR+ oriTRK2 strAB+* (suicide vector)	(Kaniga et al., 1991)
pAD208	*pKNG101-sctV-egfp*	(Diepold et al., 2017)
pAD439	*pKNG101-pamcherry1-sctD*	This work
pAD638	$pBAD::sctF_{S5C}$	This work
pEE010	$pBAD::sctD_{H193A,H205S,R214H,H353Y,H376G}$	This work
pISO85	*pKNG101-ΔsctF*	(Diepold et al., 2010)
pSW001	*pBAD::pHluorin*	This work
pSW022	*pBAD::sctD*	This work

Supplementary Table 1 – Strains and plasmids used in this study

Low salt LB medium	**concentration**
Yeast extract	5 g/l
Trypton	10 g/l
NaCl	3 g/l
Agarose (for plates)	1.5%

BHI medium	**concentration**
Brain heart infusion solids	17.5 g/l
Peptones	10.0 g/l
Glucose	2.0 g/l
Sodium chloride	5.0 g/l
Disodium hydrogen phosphate	2.5 g/l
Agarose (for plates)	1.5%

Minimal microcopy medium	**concentration**
HEPES pH 7.2	100 mM
$(NH_4)_2SO_4$, ammonium sulfate	5 mM
NaCl	100 mM
Sodium glutamate	20 mM
$MgCl_2$	10 mM
K_2SO_4	5 mM
MES	5 mM
Glycine	50mM
Casamino acids	0.5%
Agarose (for agarose pads)	1.5%

Supplementary Table 2 – Composition of media used in this study

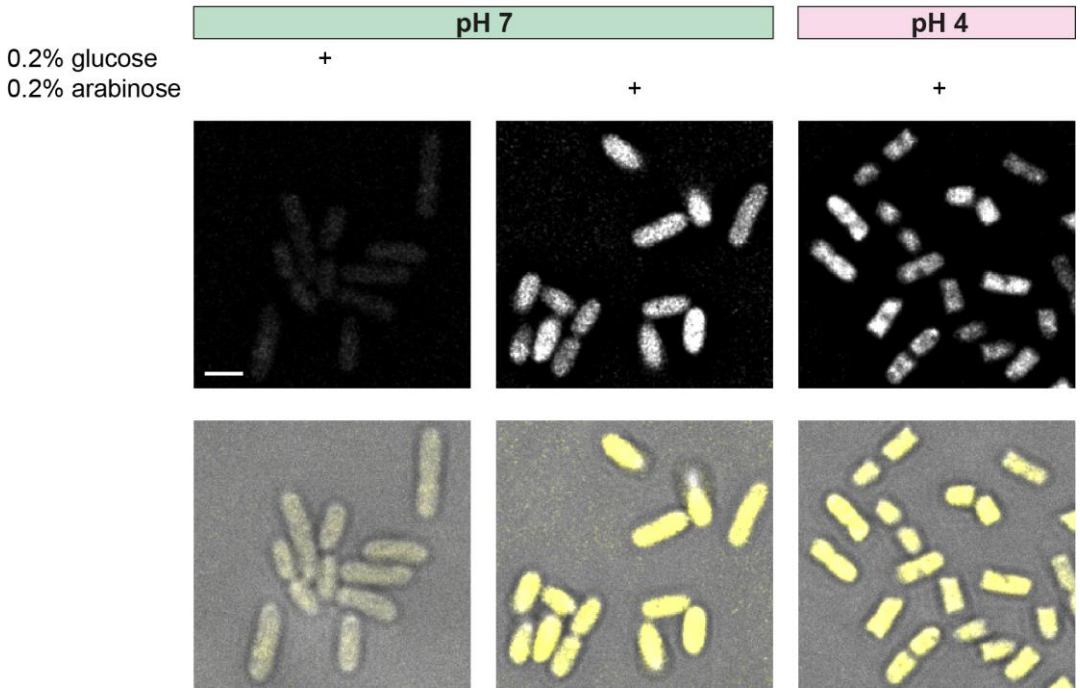

Suppl. Fig. 1 – Protein synthesis in *Y. enterocolitica* is not suppressed at an external pH of 4

Y. enterocolitica dHOPEMTasd were grown at neutral pH and then subjected to different pH as indicated. EGFP expression was induced from a pBAD plasmid at the same time, and fluorescence was determined after 180 min. Top, fluorescence image in GFP channel, bottom, overlay of phase contrast (grey) and fluorescence (yellow). Scale bar, 2 µm.

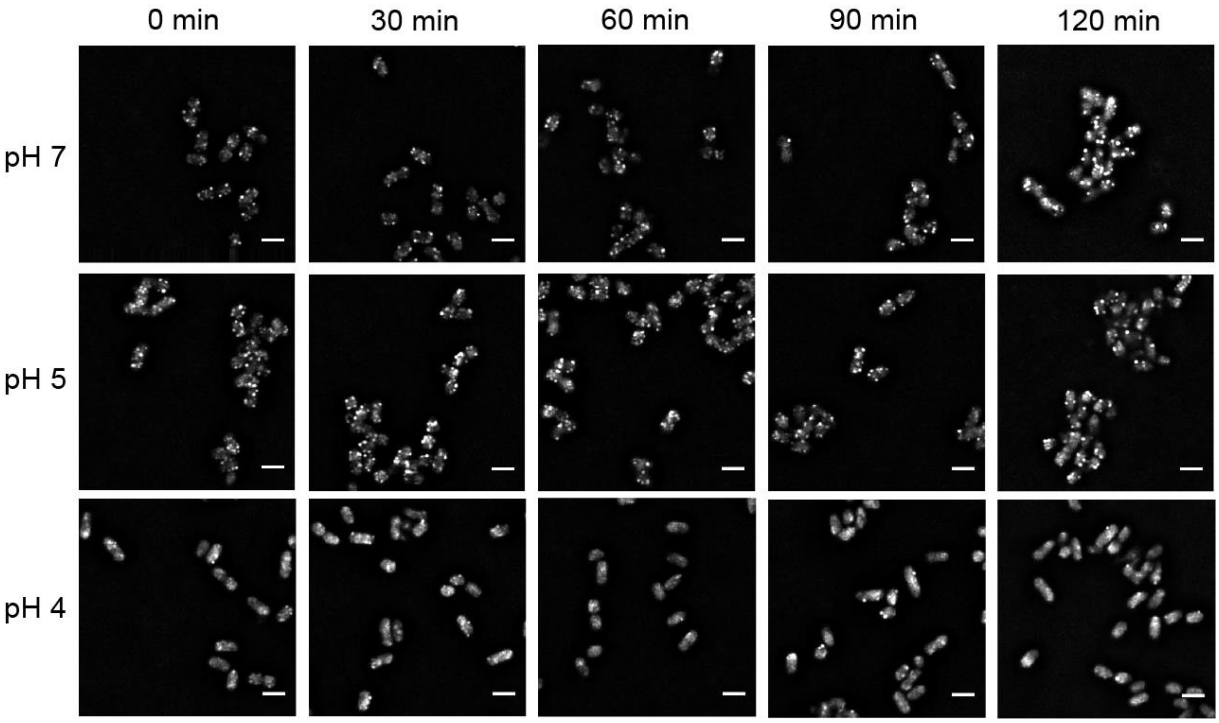

Suppl. Fig. 2 – The localization of the cytosolic components remains stable over time

Fluorescence micrographs of *Y. enterocolitica* EGFP-SctQ, incubated at the indicated external pH values under secreting conditions over time. Scale bars, 2 µm.

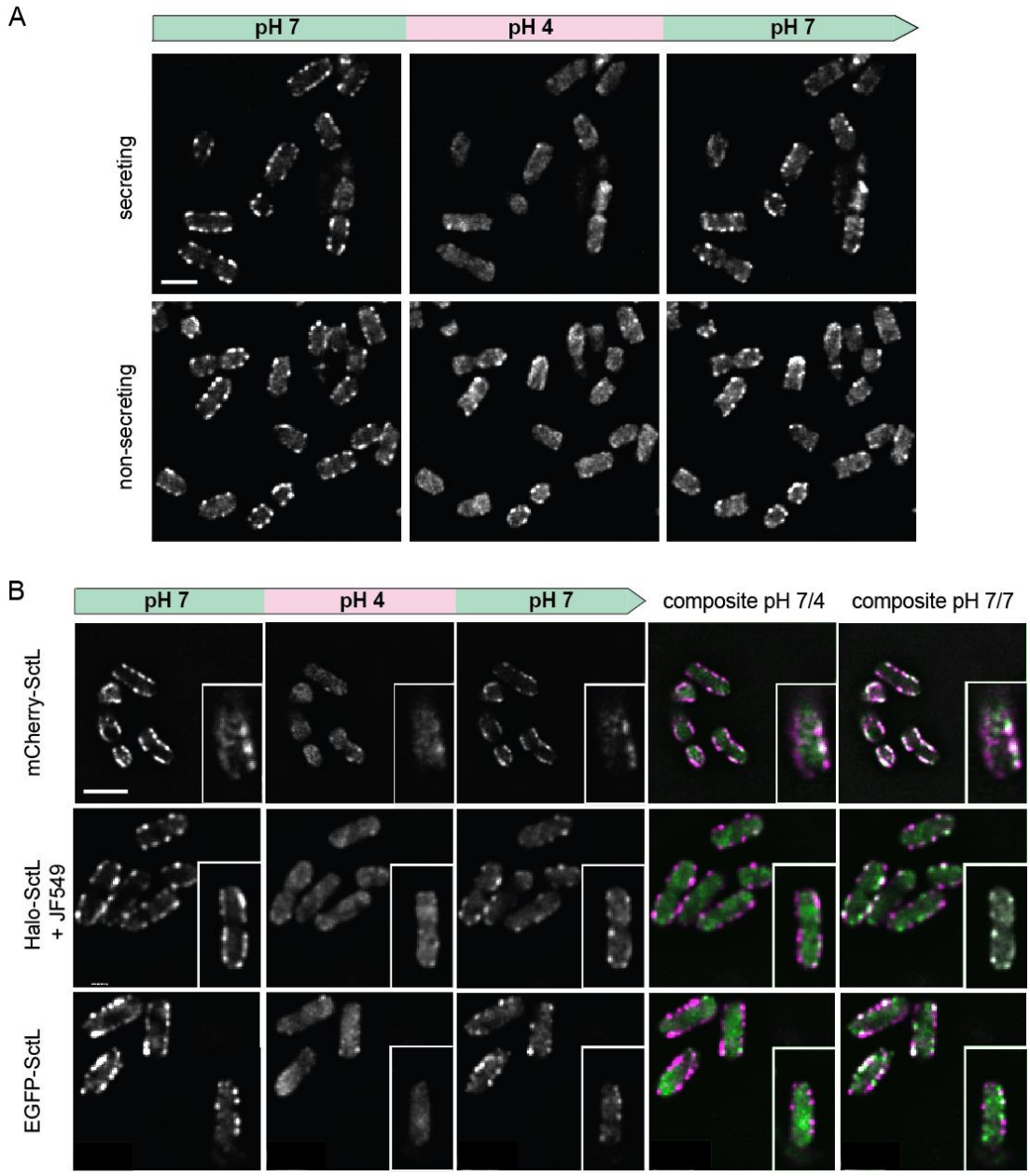

Suppl. Fig. 3 – Dissociation of the cytosolic components at low external pH can be observed irrespective of the used visualization tag, and in both secreting and non-secreting conditions

(**A**) Fluorescence micrographs of *Y. enterocolitica* EGFP-SctQ, incubated at the indicated external pH values under secreting conditions (top), or non-secreting conditions (bottom) over time. (**B**) Fluorescence micrographs of *Y. enterocolitica* expressing indicated labeled versions of SctL (replacing the WT gene by allelic exchange) at the indicated external pH values under secreting conditions over time. Right columns, composite images; magenta: pH 7 (first image on the left); green: pH 4 (second image on the left) or pH 7 (third image on the left), as indicated. Scale bars, 2 µm.

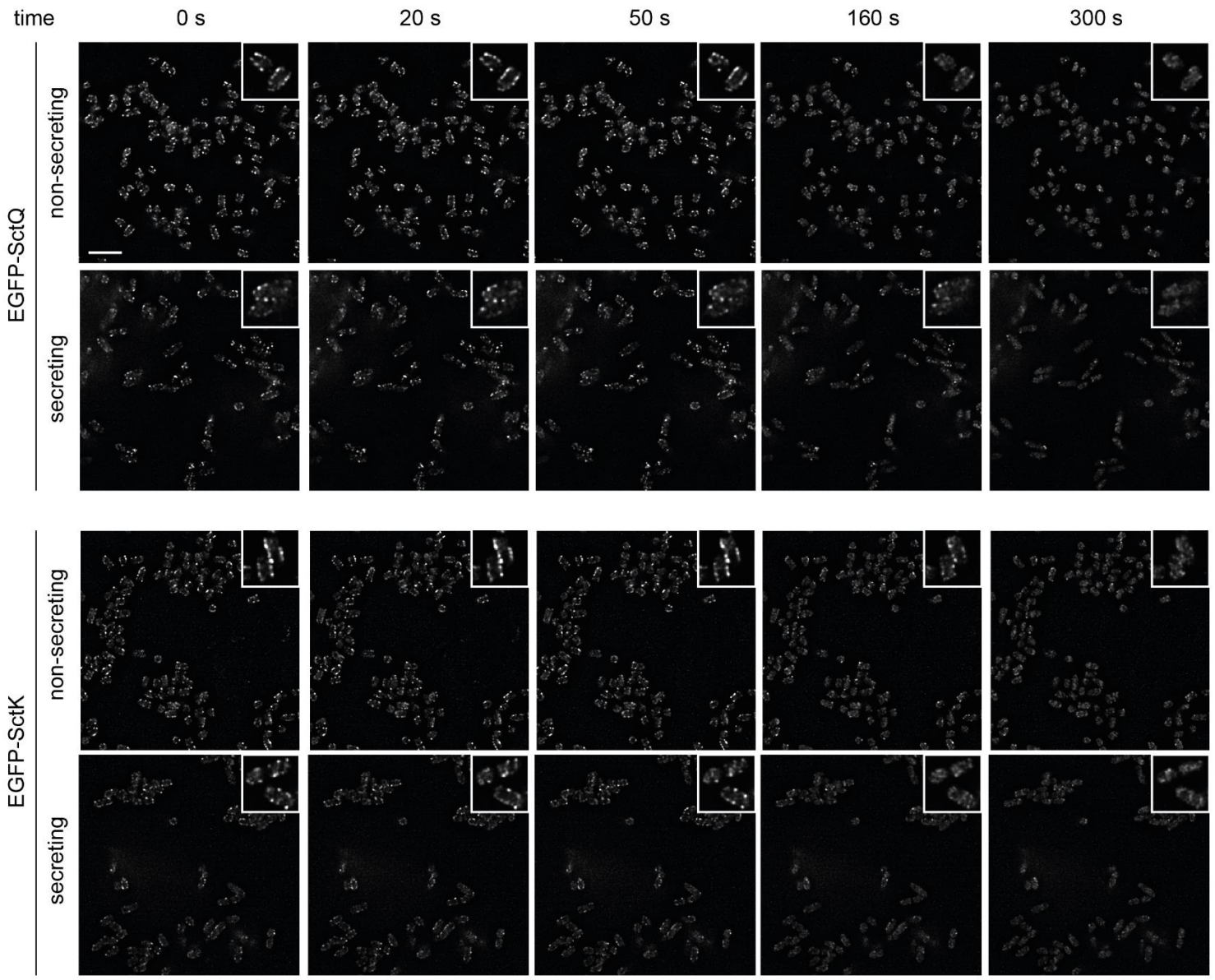

Suppl. Fig. 4 – Dissociation kinetics of the cytosolic T3SS components under secreting and non-secreting conditions

Fluorescence micrographs of *Y. enterocolitica* EGFP-SctQ (top) or EGFP-SctK (bottom), at the given time periods after subjecting the bacteria to an external pH of 4 in a flow cell, under secreting conditions (rows 1 and 3), or non-secreting conditions (rows 2 and 4) Scale bar, 5 µm; insets show enlarged sections of the micrographs.

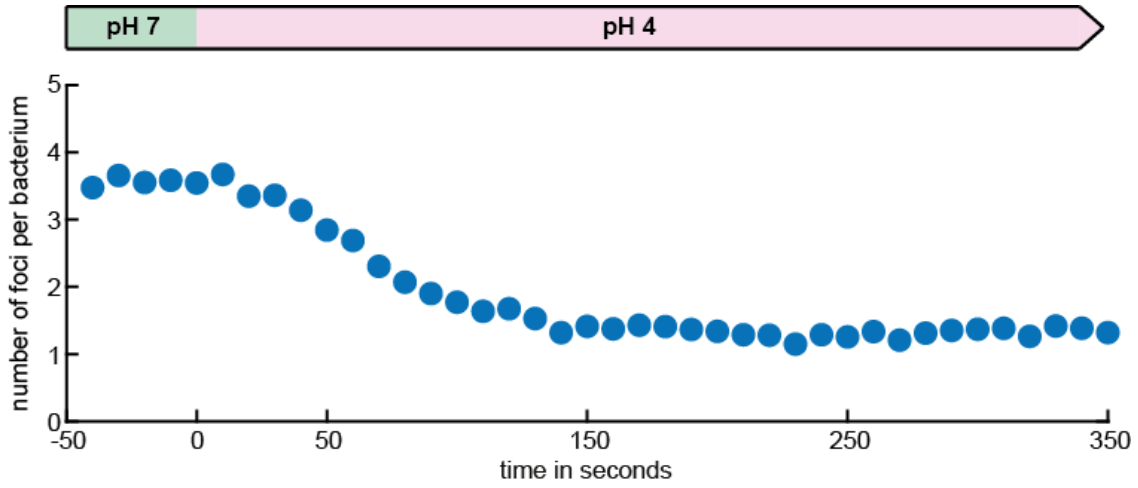

Suppl. Fig. 5: Quantification of EGFP-SctQ dissociation kinetics upon exposure to external pH 4.

The number of fluorescent EGFP-SctQ foci detected by BiofilmQ (see Material and Methods for details) was determined every 10 s in a flow cell upon changing the external pH from 7 to 4. *n* = 270 bacteria.

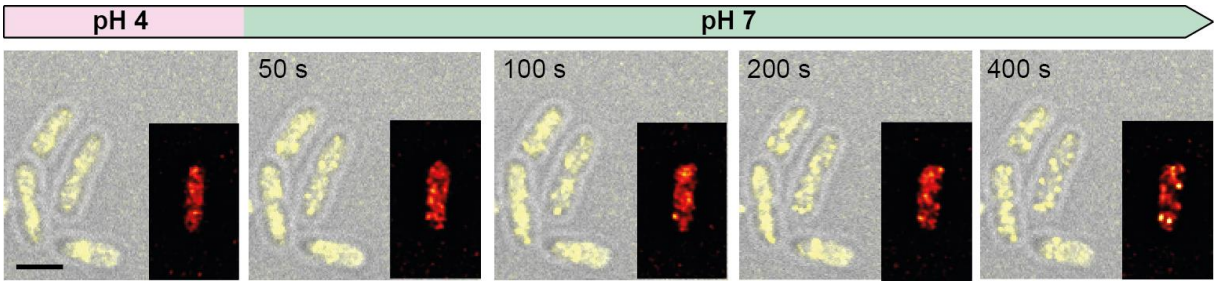

Suppl. Fig. 6: Re-association kinetics of EGFP-SctQ upon restoration of neutral external pH

Kinetics of EGFP-SctQ re-association after pH shift from 4 to 7. Overlay of phase contrast (grey) and fluorescence images (yellow); insets, enlarged single bacteria, visualized with the ImageJ red-hot color scale. Scale bar, 2 µm.

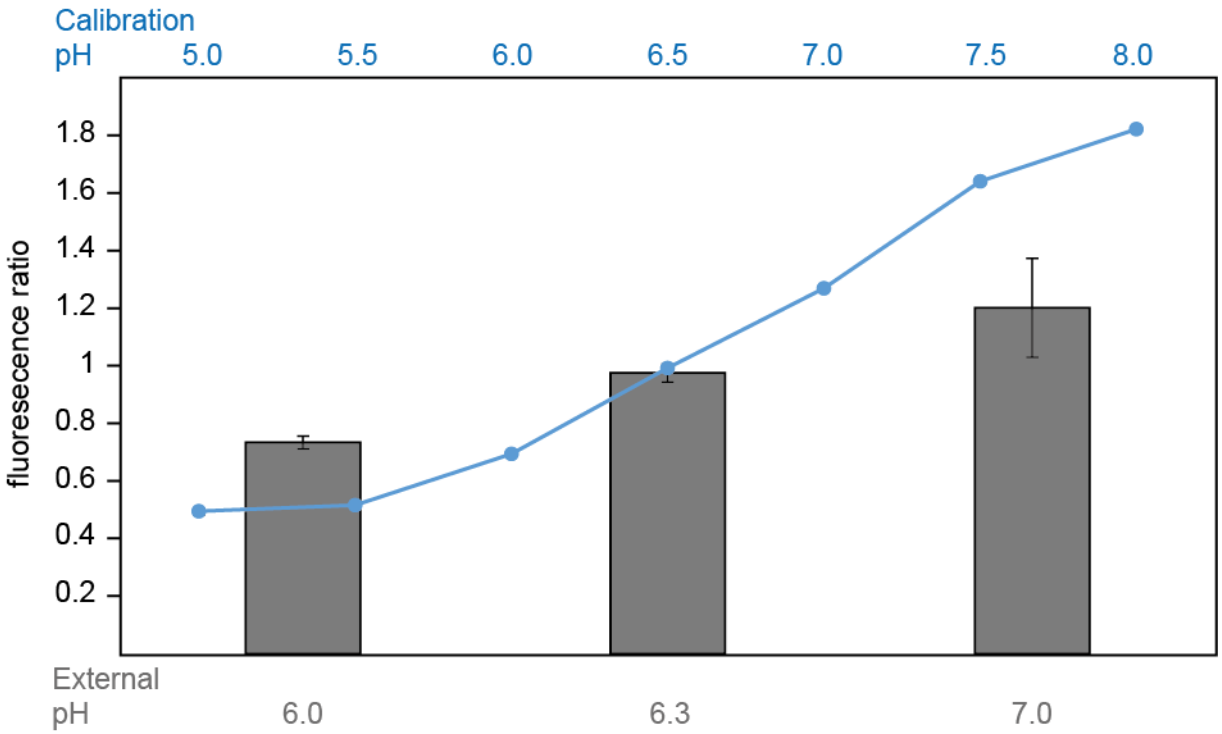

Suppl. Fig. 7: Internal pH is equilibrated with external pH upon DNP treatment

Blue curve, calibration of (Ex_{390nm} / Ex_{475nm}) fluorescence ratio of purified $pHluorin_{M153R}$ for the pH values indicated on the top (blue) (see Fig. 3A). Technical triplicate, error bars too small to display. Grey bars, determination of cytosolic pH upon incubating bacteria at the indicated external pH values (bottom) in presence of 2 mM DNP. Fluorescence ratio (Ex_{390nm} / Ex_{475nm}) of bacteria expressing cytosolic $pHluorin_{M153R}$. *n* = 3, error bars denote standard deviation.

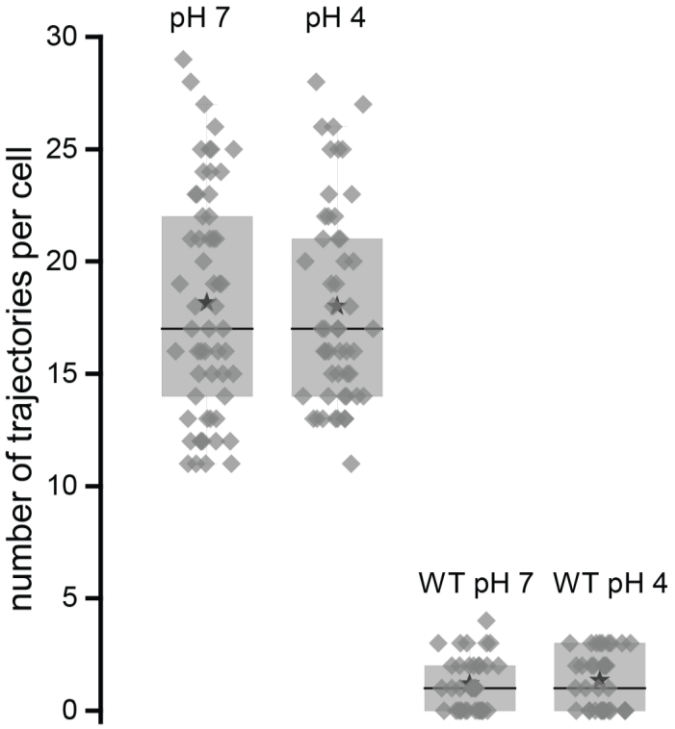

Suppl. Fig. 8 - Number of SctD trajectories in *Y. enterocolitica* cells at pH 7 and pH 4 compared to the number of false positives measured in wild type cells

Number of PAmCherry-SctD trajectories per single living *Y. enterocolitica* cells at pH 7 and at pH 4 both exhibit a medium trajectory number of 17 trajectories per cell and a mean of 18.2 ± 5.1 s.d. (pH 7) and 18.0 ± 4.4 s.d. (pH 4). As a control, strains expressing PAmCherry-SctD were mixed with wild type cells during the sample preparation. False positive trajectories from the background signal of single wild type cells in the same movies yield a median of one false positive trajectory per cell for both conditions and a mean of 1.2 ± 1.1 s.d. (pH 7) and 1.3 ± 1.2 s.d. (pH 4). Symbols in the histogram are black star mean, black line median, whisker range 5-95% and box range 25-75%.

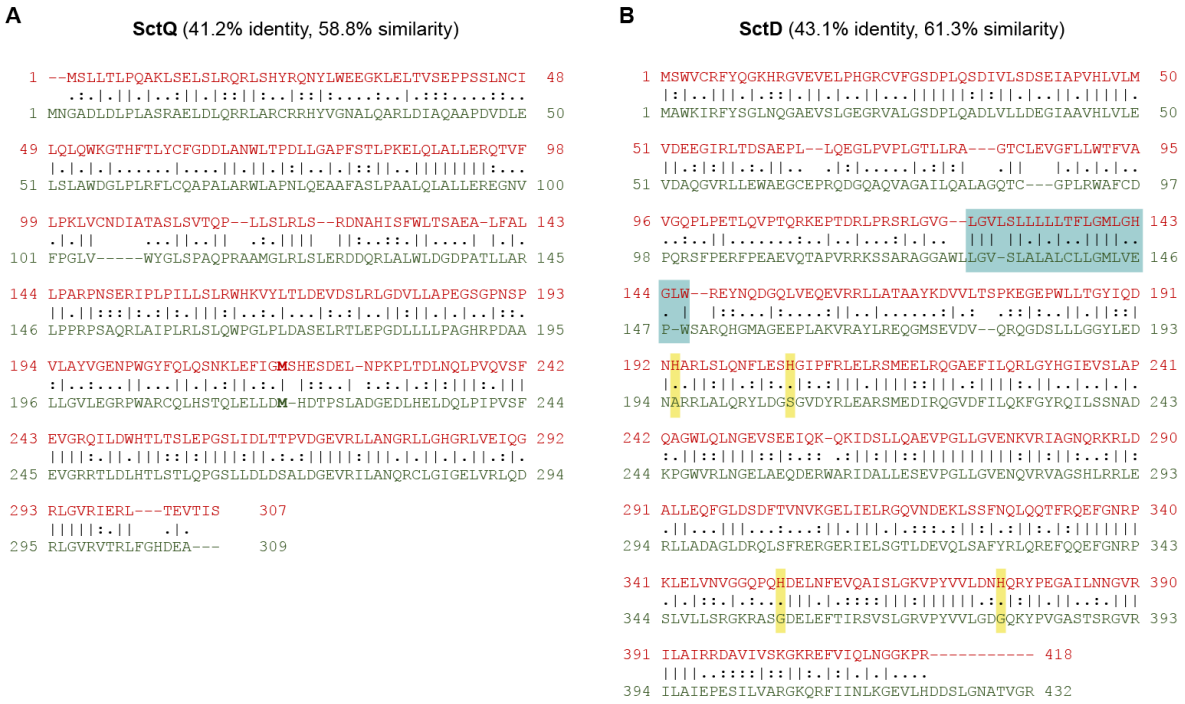

Suppl. Fig. 9 – Sequence conservation of T3SS components in *Y. enterocolitica* and *P. aeruginosa*

Pairwise sequence alignment of SctQ (**A**) and SctD (**B**). Red, *Y. enterocolitica* sequences (NP_052404, NP_052414); green *P. aeruginosa* PAO1 sequences (NP_250385, NP_250408). Alignments created with EBI EMBOSS Needle (https://www.ebi.ac.uk/Tools/psa/emboss_needle/). Bold M indicates internal translation start site of $SctQ_C$ (amino acid 218 in *Y. enterocolitica*) (Bzymek et al., 2012; Yu et al., 2011). Turquoise background indicates region of precited trans-membrane region for *Y. enterocolitica* SctD, as predicted by Phobius (Käll et al., 2007). The regions upstream and downstream of the TMH correspond to the cytosolic and periplasmic parts of the structure, respectively. Amino acids highlighted in yellow were identified as potentially important for pH sensing in SctD.

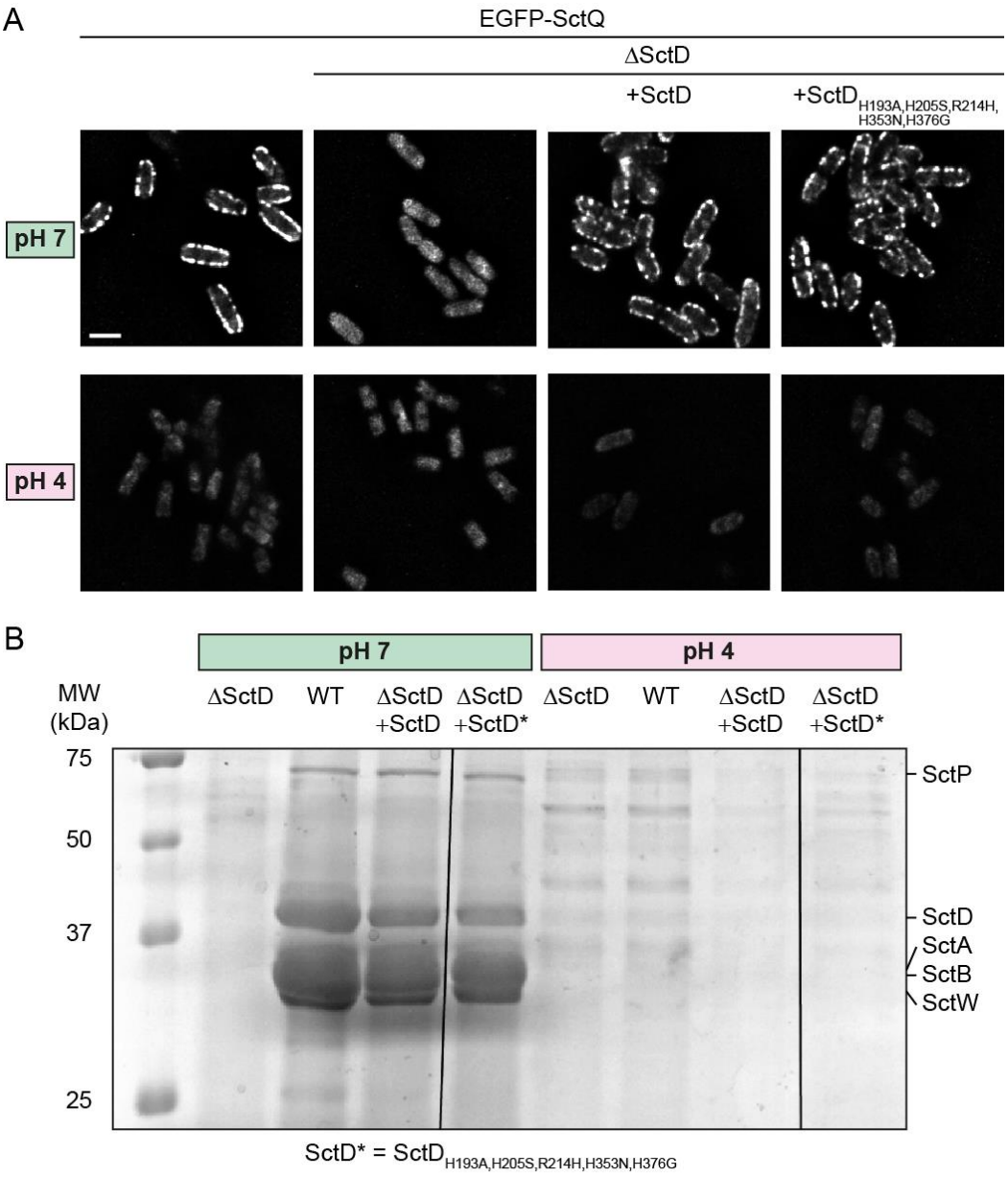

Suppl. Fig. 10 – Point mutations in SctD do no suppress the pH-dependent dissociation of cytosolic T3SS components and suppression of secretion at low external pH.

(**A**) Fluorescence micrographs of *Y. enterocolitica* EGFP-SctQ in strains lacking SctD (column 2-4) and complemented *in trans* with wild-type SctD (column 3) or an SctD multiple point mutant (see main text for details), at pH 7 (top) or pH 4 (bottom). The mutant SctD confers the same phenotype on SctQ localization as wild-type SctD under both conditions. Sclae bar, 2 µm. (**B**) *In vitro* secretion assay showing the export of native T3SS substrates in the strains used in (A), at external pH of 7 (left) or 4 (right). All samples were analyzed on the same SDS-PAGE gel, vertical lines denote the omission of intermediate lanes. Molecular weight in kDa and exported proteins are indicated and the left and right side, respectively.

Supplementary Movies

Suppl. Movie 1-2 – *Y. enterocolitica* attaches to surfaces at low external pH

Suppl. Movie 1: Time-lapse phase contrast video of *Y. enterocolitica* attached to a glass cover slip in a flow cell at pH 7. The buffer was exchanged from pH 7 to pH 4 buffered media during the experiment and cells were tracked for 10 minutes with a picture taken every 10 seconds.

Suppl. Movie 2: Time-lapse phase contrast video of *Y. enterocolitica* attached to a glass cover slip in a flow cell at pH 4. During the experiment the buffer was changed from pH 4 to pH 7 and cells were tracked again for 10 minutes with a picture taken every 10 seconds. Scale bars, 2 µm.

Suppl. Movie 3 – The pH-induced dissociation and re-association of EGFP-SctK to the injectisome can be repeated for several cycles.

Time-lapse video of *Y. enterocolitica* expressing EGFP-SctK attached to a glass cover slip in a flow cell. After flow was started the buffer was toggled every 5 minutes between pH 7 to pH 4, as indicated. Micrographs were acquired every 10 seconds. Scale bar, 2 µm.

Suppl. Movie 4 – Dissociation kinetics of EGFP-SctQ upon change of external pH from 7 to 4

Time-lapse video of *Y. enterocolitica* expressing EGFP-SctQ attached to a glass cover slip in a flow cell after pH shift from 7 to 4. Left, overlay of DIC (grey) and fluorescence signal (yellow); right, fluorescent channel in red hot color scale. Bacteria were attached to the cover slip at pH 7, flow was introduced, and the buffer was switched from pH 7 to pH 4. The duration of the experiment was 10 minutes and pictures were taken every 10 seconds. Scale bar, 2 µm.

Suppl. Movie 5 – Re-association kinetics of EGFP-SctQ upon change of external pH from 4 to 7

Time-lapse video of *Y. enterocolitica* expressing EGFP-SctQ attached to a glass cover slip in a flow cell after pH shift from 4 to 7. Left, overlay of DIC (grey) and fluorescence signal (yellow); right, fluorescent channel in red hot color scale. Bacteria were attached to the cover slip at pH 7, flow was introduced, and the buffer was switched from pH 4 to pH 7. The duration of the experiment was 10 minutes and pictures were taken every 10 seconds. Scale bar, 2 µm.

Supplementary references

Bzymek KP, Hamaoka BY, Ghosh P. 2012. Two translation products of Yersinia yscQ assemble to form a complex essential to type III secretion. *Biochemistry* **51**:1669–77. doi:10.1021/bi201792p

Diepold A, Amstutz M, Abel S, Sorg I, Jenal U, Cornelis GR. 2010. Deciphering the assembly of the Yersinia type III secretion injectisome. *EMBO J* **29**:1928–1940. doi:10.1038/emboj.2010.84

Diepold A, Kudryashev M, Delalez NJ, Berry RM, Armitage JP. 2015. Composition, Formation, and Regulation of the Cytosolic C-ring, a Dynamic Component of the Type III Secretion Injectisome. *PLOS Biol* **13**:e1002039. doi:10.1371/journal.pbio.1002039

Diepold A, Sezgin E, Huseyin M, Mortimer T, Eggeling C, Armitage JP. 2017. A dynamic and adaptive network of cytosolic interactions governs protein export by the T3SS injectisome. *Nat Commun* **8**:15940. doi:10.1038/ncomms15940

Käll L, Krogh A, Sonnhammer ELL. 2007. Advantages of combined transmembrane topology and signal peptide prediction--the Phobius web server. *Nucleic Acids Res* **35**:W429-32. doi:10.1093/nar/gkm256

Kaniga K, Delor I, Cornelis GR. 1991. A wide-host-range suicide vector for improving reverse genetics in Gram-negative bacteria: inactivation of the blaA gene of Yersinia enterocolitica. *Gene* **109**:137–141. doi:10.1016/0378-1119(91)90599-7

Kudryashev M, Stenta M, Schmelz S, Amstutz M, Wiesand U, Castaño-Díez D, Degiacomi MTM, Münnich S, Bleck CKC, Kowal J, Diepold A, Heinz DWD, Dal Peraro M, Cornelis GR, Stahlberg H. 2013. In situ structural analysis of the Yersinia enterocolitica injectisome. *Elife* **2**:e00792. doi:10.7554/eLife.00792

Sory M-P, Boland A, Lambermont I, Cornelis GR. 1995. Identification of the YopE and YopH domains required for secretion and internalization into the cytosol of macrophages, using the cyaA gene fusion approach. *Proc Natl Acad Sci U S A* **92**:11998–12002.

Yu X-J, Liu M, Matthews S, Holden DW. 2011. Tandem translation generates a chaperone for the Salmonella type III secretion system protein SsaQ. *J Biol Chem* **286**:36098–107. doi:10.1074/jbc.M111.278663